Damage Assessment Based on the Frequencies' Ratio Surfaces Intersection Method for the Identification of the Crack Depth, Location and Orientation

Jean-Jacques Sinou

Damage Assessment Based on the Frequencies' Ratio Surfaces Intersection Method for the Identification of the Crack Depth, Location and Orientation

Jean-Jacques Sinou[1]

Abstract: This paper aims to establish a damage identification methodology, called the Frequencies' Ratio Surfaces Intersection method (FRSI-method), for predicting not only the location and depth of the crack but also the crack orientation in a circular cross section beam. Two new criterions $\%\Delta_i^{cracked}$ and $\%\Psi_{i,j}^{cracked}$ that consider only the ratio of the natural frequencies of the cracked beam are introduced and discussed in order to detect the crack parameters. In order to avoid worse diagnostic, it is demonstrated that a robust identification of crack location is possible by investigating the emergence of extra antiresonance peaks on Frequency Response Functions.
The size, location and orientation of the crack are identified by finding the intersection of the surfaces that correspond to the natural frequencies' ratios of the lower vertical and horizontal modes. One of the advantages of the proposed approach is that, unlike other vibration-based damage identification procedures, it does not use a priori accurate knowledge of the angular frequencies of the uncracked structure and its material properties. Only the Frequency Responses Functions and natural frequencies of the cracked structure are needed to identify the crack parameters (i.e. the non-dimensional crack depth, the crack location and the crack orientation).
It is demonstrated that damage identification methodology, called the Frequencies' Ratio Surfaces Intersection method (FRSI-method), can be used for the detection of the crack size, location and orientation with satisfactory precision, even if noise level has been added to the simulations.

keyword: damage detection, vibration, frequencies and antiresonances, identification of the crack size, location and orientation, uncertainties.

[1] Corresponding author. Laboratoire de Tribologie et Dynamique des Systèmes UMR-CNRS 5513, Ecole Centrale de Lyon, 36 avenue Guy de Collongue, 69134 Ecully Cedex, France. jean-jacques.sinou@ec-lyon.fr

1 Introduction

For many years, vibration of cracked structures and damage identification methods have been studied by a number of researchers. Dimarogonas (Dimarogonas 1996), Doebling et al. (Doebling et al. 1998) and Wauer (Wauer 1990) gave a review of the research on vibration of cracked structures and damage detection and location using vibration data.

A variety of methods has been developed to identify the crack size and location. These approaches are mainly based on the change in modal properties of cracked structures (Adams et al. 1978; Morassi 1993; Hearn and Testa 1991; Liang 1992; Cerri and Vestroni 2000; Khiema and Lien 2004), the damage-induced shifts in the first natural frequencies and the corresponding amplitudes (Owolabi et al. 2003), the mode shapes variation due to the presence of the crack, and force response measurements (Dharmaraju et al. 2002; Dharmaraju et al. 2004). For example, some researchers proposed to consider the point of intersection of contour lines that correspond to the frequency changes in terms of the non-dimensional crack depth and location (Nahvi and Jabbari 2005; Li et al. 2005; Owolabi et al. 2003; Swamidas et al. 2004). In these studies, the identification of the crack size and location is possible under the situation that measured natural frequencies of crack beams are set as input.
Recently, Dilena and Morassi (Dilena and Morassi 2002) and Gladwell and Morassi (Gladwell and Morassi 1999) proposed a damage identification based on the changes in the nodes of mode shapes. Then they demonstrated that an appropriate use of resonances and antiresonances may be used in order to avoid the non-uniqueness of the damage location for symmetrical beams (Dilena and Morassi 2004). Bamnious et al (Douka et al. 2004; Bamnios et al. 2002) proposed a simplified method for detecting crack size and location. They used the shift in the antiresonances of the

cantilever cracked beam. Moreover, they indicated that the driving-point mechanical impedance changes not only due to the crack size and location but also the force location. It may be noted that the importance and significance of antiresonances in experimental structural analysis was previously investigated by Wahl et al.(Wahl et al. 1996). Even if Dharmaraju and Sinha (Dharmaraju and Sinha 2005) demonstrated that the identification of the crack location due to the change in antiresonance could be difficult, they concluded that a more robust identification based on the previous methodology has to be developed for practical applications.

The purpose of the present work is to establish a new methodology for predicting not only the location and depth of a crack in a circular cross section beam, but also the crack orientation. Moreover, the objective of this research is to demonstrate that the knowledge of the natural frequencies of the cracked beam is sufficient in order to identify all the crack parameters (i.e. the non-dimensional crack depth, the crack location and the crack orientation). So, two new criterions ($\%\Delta_i^{cracked}$ and $\%\Psi_{i,j}^{cracked}$) will be introduced and discussed in order to undertake the damage identification without needing an accurate knowledge of the material propoerties (i.e. the Young's modulus and the density), and the values of the natural frequencies of the uncracked structure. Then, an extension of the frequency contour lines method, called Frequencies' Ratio Surfaces method (FRS-method) will be developed in order to obtain a robust detection of crack size, location and orientation in beams. Finally, in order to avoid the non-uniqueness of the damage location problem due to the structural symmetry of structures, the emergence of antiresonances on the Frequency Response Functions is used.

The paper is set up as follows: first the model of the crack beam is given and the effects of the crack parameters (the non-dimensional crack depth, the crack orientation and the crack location) are briefly investigated in order to explain the possible coupling of the two lateral bending vibrations due to the presence of a transverse crack. Secondly, the damage identification technique based on the Frequencies' Ratio Surfaces Intersection method (FRSI-method) and the criterion $\%\Delta_i^{cracked}$ that allows the identification of the crack size, orientation and location is presented. Finally, an extension of the previous criterion (the generalized criterion $\%\Psi_{i,j}^{cracked}$) is introduced in order to allow the detection of the crack parameters for complex structures. The efficiency and robustness of the proposed identification technique is demonstrated through numerical simulations corresponding to different non-dimensional crack depths, crack orientations and crack locations without noise and when uniform random noise is added to the numerical simulations.

2 The model of the simply supported cracked beam and the effects of cracks

In this section, details of the crack model and the complete modeling of the system are firstly presented. Secondly, the effects of a transverse crack on the two lateral bending vibrations and shift in the resonances of the cracked beam are briefly discussed.

2.1 Crack model

A circular cross section beam that is simply supported at each end is studied. The physical parameters of the beam are given in Table 1.

The beam element has been discretized into 30 Euler-Bernouilli beam finite elements with four degrees of freedoms at each node (Nelson and Nataraj 1986; Lalanne and Ferraris 1990), as illustrated in Figure 1.

The presence of a transverse surface crack on the circular beam introduces a local flexibility due to strain energy concentration in the vicinity of the crack tip under load. Mayes and Davies (Davies and Mayes 1984; Mayes and Davies 1984) proposed to theoretically model a transverse crack by reducing the second moment of area of the element at the location of the crack by ΔI

$$\Delta I = I_0 \left(1 + \left(\frac{R}{l} \left(1 - \nu^2\right) F(\mu) \right)^{-1} \right) \tag{1}$$

where I_0, R , l, and ν are the second moment of area, the shaft radius, the length of the section and the Poisson's ratio, respectively. μ is the non-dimensional crack depth and is given by $\mu = \frac{h}{R}$ where h defines the crack depth of the shaft, as illustrated in Figure 1. $F(\mu)$ is the non-linear compliance functions that can be obtained from a series of experiments with chordal cracks (Davies and Mayes 1984; Mayes and Davies 1984). For convenience, let the principal η-axis be aligned with the crack front. The moments of inertia about the parallel centroidal axes, I_η and I_ξ, are given by

(Sinou and Lees 2005)

$$I_\eta = \frac{R^4}{4}\left((1-\mu)\left(1-4\mu+2\mu^2\right)\gamma+\frac{\alpha}{2}\right) \quad (2)$$

$$I_\xi = R^4\left(\frac{\pi}{4}+(1-\mu)\gamma\left(\frac{2\gamma^2}{3}+\frac{1-4\mu+2\mu^2}{4}\right) + sin^{-1}(\gamma)-\frac{4}{9}\left((1-\mu)\gamma+\frac{\alpha}{2}\right)^{-1}\gamma^6\right) \quad (3)$$

where R is the shaft radius, μ is the crack depth, and $\gamma = \sqrt{2\mu-\mu^2}$ for convenience. α is the crack angle (as shown in Figure 1). It may be observed that the change of I_0 on the axis ξ is relatively small in comparison to the change on the axis η (Gasch 1993; Sinou and Lees 2005).

Then, the stiffness matrix due to the transversal crack $\mathbf{K}_{crack}^{\eta,\xi}$ can be obtained at the crack location in η and ξ coordinate axis, by using standard finite elements (Nelson and Nataraj 1986; Lalanne and Ferraris 1990). The matrice $\mathbf{K}_{crack}^{\eta,\xi}$ for a two node Timoshenko beam element of length l and Young's modulus E corresponding to the dof vector $[u_1 \quad v_1 \quad \theta_1 \quad \psi_1 \quad u_2 \quad v_2 \quad \theta_2 \quad \psi_2]$, as shown in Figure 1, can be written as below

$$\mathbf{K}_{crack}^{\eta,\xi} = \frac{E}{l^3}\begin{bmatrix} 12I_\eta & 0 & 0 & 6lI_\eta & -12I_\eta & 0 & 0 & 6lI_\eta \\ & 12I_\xi & -6lI_\xi & 0 & 0 & -12I_\xi & -6lI_\xi & 0 \\ & & 4l^2I_\xi & 0 & 0 & 6lI_\xi & 2l^2I_\xi & 0 \\ & & & 4l^2I_\eta & -6lI_\eta & 0 & 0 & 2l^2I_\eta \\ & & & & 12I_\eta & 0 & 0 & -6lI_\eta \\ & & & & & 12I_\xi & 6lI_\xi & 0 \\ & & Sym. & & & & 4l^2I_\xi & 0 \\ & & & & & & & 4l^2I_\eta \end{bmatrix} \quad (4)$$

Consequently, the stiffness matrix in X and Y coordinate axis is given by

$$\mathbf{K}_{crack} = diag\left(\mathbf{P}^T\ \mathbf{P}^T\ \mathbf{P}^T\ \mathbf{P}^T\right) \times \mathbf{K}_{crack}^{\eta,\xi} \times diag\left(\mathbf{P}\ \mathbf{P}\ \mathbf{P}\ \mathbf{P}\right) \quad (5)$$

where $\mathbf{P}$ is given by

$$\mathbf{P} = \begin{bmatrix} cos\chi & sin\chi \\ -sin\chi & cos\chi \end{bmatrix} \quad (6)$$

χ defines the angle between the orientation of the crack front and the vertical X-axis, as shown in Figure 1.

2.2 System equation of motion

The equation of motion for the simply supported cracked beam can be written as

$$\mathbf{M}\ddot{\mathbf{X}} + \mathbf{C}\dot{\mathbf{X}} + \tilde{\mathbf{K}}\mathbf{X} = \mathbf{F}(t) \quad (7)$$

where $\mathbf{X}$ is the vector of nodal degrees of freedom of the system. t defines the time instant. $\mathbf{M}$ is the mass matrix, $\tilde{\mathbf{K}}$ is the global stiffness matrix, $\mathbf{F}(t)$ is the external force vector, and dot represents the derivative with respect to the time. $\mathbf{C}$ defines the proportional damping matrix and can be expressed as $\mathbf{C} = \alpha\mathbf{M} + \beta\mathbf{K}$ (with α and β real constants). $\tilde{\mathbf{K}}$ contains the stiffness reduction $\mathbf{K}_{crack}$ at the crack location .

Let the force vector be defined as $\mathbf{F}(t) = \mathbf{F_0}e^{i\omega t}$ where ω is the forcing frequency, and $\mathbf{F_0}$ defines the force amplitude vector. Therefore, the response vector may be assumed as $\mathbf{X}(t) = \mathbf{X_0}e^{i\omega t}$ and Equation 7 is given by

$$\left(-\omega^2\mathbf{M} + i\omega\mathbf{C} + \tilde{\mathbf{K}}\right)\mathbf{X_0} = \mathbf{F_0} \quad (8)$$

Due to the fact that $\tilde{\mathbf{K}}$ contains the contribution of the crack $\mathbf{K}_{crack}$ at the cracked element degrees-of-freedom and the assembled stiffness matrix of the uncracked beam, the previous equation may be rewritten as

$$\left(-\omega^2\mathbf{M} + i\omega\mathbf{C} + \mathbf{K}\right)\begin{bmatrix} \mathbf{X_0}^c \\ \mathbf{X_0}^{uc} \end{bmatrix} = \mathbf{F_0} - \mathbf{F_c} = \begin{bmatrix} \mathbf{F_0}^c \\ \mathbf{F_0}^{uc} \end{bmatrix} - \begin{bmatrix} \mathbf{F_c}^c \\ \mathbf{0} \end{bmatrix} \quad (9)$$

where $\mathbf{K}$ defines the stiffness matrix of the uncracked system. The subscripts c and uc represent the cracked and uncracked elements, respectively. $\mathbf{F_0}$ contains the external force vector, and $\mathbf{F_c}$ represents the force vector only due to the contribution of the crack. It may be observed that the vector $\mathbf{F_c}$ contains non-zero terms only at the crack nodal degrees of freedom and $\mathbf{F_c}^c$ is given by

$$\mathbf{F_c}^c = \mathbf{K}_{crack}\mathbf{X_0}^c \quad (10)$$

2.3 Effects of crack on the lateral bending vibrations

The objective of this section is to explain the possible coupling of the two lateral vibrations due to the presence of cracks. The role of cracks on the two lateral vibrations of the cracked beam will be used in the following parts of the paper in order to avoid the non-uniqueness of the crack location.

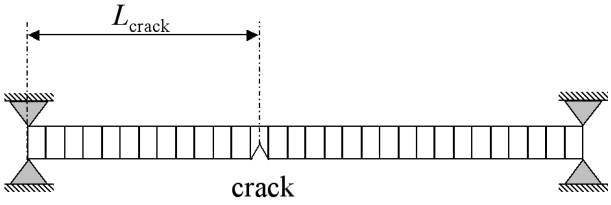

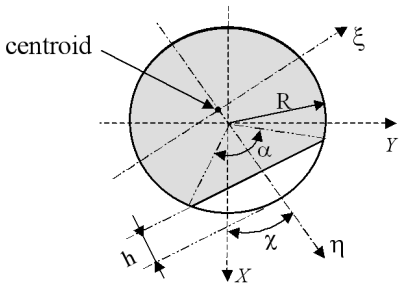

(a) Geometry of the cracked-beam section

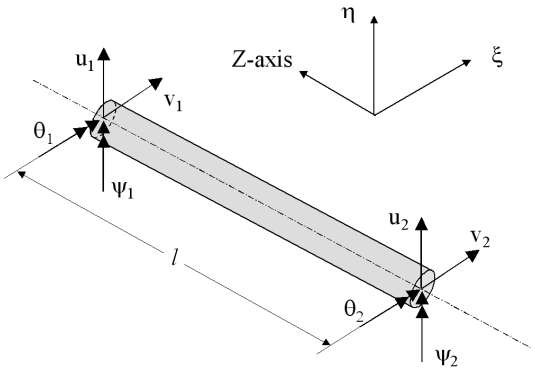

(b) Description of the Dof in the ξ-η axis

Figure 1 : Finite-element model

Table 1 : Physical parameters of the beam

Notation	Description	Value
R	radius of the rotor shaft	$0.05m$
L	length of the rotor shaft	$1m$
E	Young's modulus of elasticity	$2.1\ 10^{11} N.m^{-2}$
ρ	density	$7800 kg.m^{-3}$
ν	Poisson ratio	0.3
β	coefficient of damping	$2\ 10^{-6}$
α	coefficient of damping	0.32
f_1, f_2	first and second frequencies of the uncracked rotor	$198.85Hz$
f_3, f_4	third and fourth frequencies of the uncracked rotor	$795.4Hz$
f_5, f_6	fifth and sixth frequencies of the uncracked rotor	$1789.66Hz$

Assuming modal viscous damping and using the normal mode substitution $\mathbf{X} = \tilde{\mathbf{\Phi}}\mathbf{q} = \sum_{r=1}^{n} q_r \tilde{\mathbf{\Phi}}_r$, the equation set 7 is diagonalized as follows:

$$\forall r \qquad \left(\tilde{\omega}_r^2 - \omega^2 + 2i\zeta_r \tilde{\omega}_r \omega\right) q_r = f_r \tag{11}$$

where f_r is the generalized modal force (i.e. $f_r = \frac{\tilde{\mathbf{\Phi}}_r^T \mathbf{F}}{m_r}$ with $m_r = \tilde{\mathbf{\Phi}}_r^T \mathbf{M} \tilde{\mathbf{\Phi}}_r$). $\tilde{\omega}_r$ is the r^{th} mode undamped natural frequency of the cracked beam ($\tilde{\omega}_r = \sqrt{\frac{\tilde{k}_r}{m_r}}$ with $\tilde{k}_r = \tilde{\mathbf{\Phi}}_r^T \tilde{\mathbf{K}} \tilde{\mathbf{\Phi}}_r$). ζ_r is the r^{th} mode damping ratio ($\zeta_r = \frac{c_r}{2 m_r \omega_r}$ with $c_r = \alpha m_r + \beta k_r$ due to the orthogonality property of $\mathbf{M}$ and $\tilde{\mathbf{K}}$; here $\omega_r = \sqrt{\frac{k_r}{m_r}}$ is the r^{th} undamped natural frequency of the uncracked beam; $k_r = \mathbf{\Phi}_r^T \mathbf{K} \mathbf{\Phi}_r$ where $\mathbf{K}$ defines the stiffness matrix of the uncracked system; and $\mathbf{\Phi}_r$ is the eigenvectors of the uncracked beam).
Finally, the relationship between the ouput vector $\mathbf{X}(\omega)$ and the input vector $\mathbf{F}(\omega)$ is given by

$$\mathbf{X}(\omega) = \mathbf{H}(\omega)\mathbf{F}(\omega) = \sum_{r=1}^{n} \frac{\tilde{\mathbf{\Phi}}_r \tilde{\mathbf{\Phi}}_r^T}{m_r \left(\tilde{\omega_r^2} - \omega^2 + 2i\zeta_r \tilde{\omega}_r \omega \right)} \mathbf{F}(\omega) \quad (12)$$

where $\mathbf{H}(\omega)$ defines the Frequency Response Function matrix. $\mathbf{H}(\omega)$ is the linear combination of each mode. Thereby, the Frequency Response Function $H_{kl}(\omega)$ (i.e. the excitation force is only applied at the l^{th} degree of freedom and the response is located at the k^{th} degree of freedom) is given by

$$H_{kl}(\omega) = \sum_{r=1}^{n} \frac{\tilde{\Phi}_{lr} \tilde{\Phi}_{kr}}{m_r \left(\tilde{\omega_r^2} - \omega^2 + 2i\zeta_r \tilde{\omega}_r \omega \right)} \quad (13)$$

Considering Equation 11, it clearly appears that the crack induces shifts in the natural frequencies of the beam due to the stiffness change. Moreover, the amplitude of the resonance peaks are affected by the crack size and crack location due to the fact that $\tilde{\omega}_r$ and $\tilde{\mathbf{\Phi}}_r$ are functions of the crack properties.

Equation 13 may be expressed by rearranging the equation of motion and extracting the force vector due to the contribution of the crack (see Equations 9 and 10). We obtain

$$\mathbf{X}(\omega) = \sum_{r=1}^{n} \frac{\tilde{\mathbf{\Phi}}_r \tilde{\mathbf{\Phi}}_r^T}{m_r (\omega_r^2 - \omega^2 + 2i\zeta_r \omega_r \omega)} \mathbf{F_0}(\omega) - \sum_{r=1}^{n} \frac{\tilde{\mathbf{\Phi}}_r \tilde{\mathbf{\Phi}}_r^T}{m_r (\omega_r^2 - \omega^2 + 2i\zeta_r \omega_r \omega)} \mathbf{F_c}(\mathbf{X}, \omega) \quad (14)$$

where $\omega_r = \sqrt{\frac{k_r}{m_r}}$ is the r^{th} undamped natural frequency of the uncracked beam.

Considering Equation 14, the possible coupling of the two lateral vibrations due to the crack can be clearly explained. The first term of Equation 14 corresponds to the effect of the external force $\mathbf{F}(t) = \mathbf{F_0} e^{i\omega t}$ where ω is the forcing frequency. The second term of Equation 14 indicates the role of the crack in order to induced vibrations. First of all, if the external force is on the direction of the crack front (i.e. on the principal η-axis), no coupling between the two lateral vibrations is observed. Effectively, the first term of Equation 14 induces only vibrations in the direction of the external force. Then, the term $\mathbf{F_c}(\mathbf{X}, \omega)$ introduces only excitation force in the same direction (see Equations 4-6, 9 and 10). Thereby, the crack does not induce excitation on the principal ξ-axis. So no vibration on the ξ-axis exists, and there is no coupling between the two lateral vibrations (on the principal ξ-axis and η-axis).
Now, the case of an external force situated on the vertical direction will be considered in order to explain the coupling between the two lateral vibrations. If the crack is fully or partially open and the crack front is different from the vertical X-axis (i.e. the external force is not on the same direction than the crack front), $\mathbf{F_c}(\mathbf{X}, \omega)$ introduces an excitation force due to the crack on the horizontal Y-axis. Consequently, the second term of Equation 14 indicates that new peaks appear on the horizontal Y-axis and vertical X-axis corresponding to the natural frequencies of the horizontal modes. Moreover, resonances peaks on the Y-axis corresponding to the natural frequencies of the vertical modes appear. This indicates the coupling of two lateral vibrations that may be observed on the horizontal and vertical axis.

2.4 Illustrations of the crack effects

In this section, numerical studies will be investigated in order to illustrate the previous explanations and the effects of the crack size, the crack location and the crack orientation. We consider a sinusoidal excitation at $0.167m$ from the left end of the simply supported beam in the vertical direction. First of all, Figures 2 illustrate the vertical and horizontal displacements of the uncracked and cracked beams as a function of the crack front orientation. As explained in the previous section, no coupling between the two lateral vibrations is observed if the crack front orientation and the direction of the external force are the same. Then if the crack is fully or partially opened (and the orientation of the crack

front is not equal to $0\,rad.$), there are new resonances on the two lateral axis (for the vertical and horizontal displacements). They correspond to the natural frequencies of the original vertical and horizontal modes. This indicates the coupling of the two lateral horizontal and vertical vibrations due to the presence of the crack.
Secondly, Figures 3 and 4 illustrate the vertical and horizontal displacements of the cracked beams as a function of the crack depth and the crack location, respectively (with the orientation of the crack front $\chi = \frac{1}{3}\pi$). If the crack location is close to the mode shape nodes, the associated modes are not greatly affected and the coupling for these modes is not clearly observed on the vertical and horizontal directions. Considering Figures 2, 3 and 4, the crack size, the crack location and the crack orientation influence the shift of the resonances and antiresonances. Moreover, this could be easily observed that the decrease in the resonances is greatest for a crack located where the bending moment is greatest. Therefore, the changes in frequencies and coupling of the two lateral vibrations appear to be not only a function of crack depth, crack location, and crack front orientation but also of the mode number.

3 The Frequencies' Ratio Surfaces Intersection method (FRSI-method)

3.1 Crack identification based on an extension of the frequency contour lines method: the Frequencies' Ratio Surfaces Intersection method

Many researchers proposed to detect the position and size of cracks by considering the first three changes in the natural frequencies of a cracked beam. Some used the intersection of the three contour lines of the first three natural cracked frequencies that indicates the possible crack position and crack size (Li et al. 2005). This methodology is only based on a careful evaluation of the cracked natural frequencies and so requires the knowledge of the material properties (the Young's modulus E and the density ρ). Others proposed to take into account the intersection of the three contour lines of the lower order normalized frequencies that are given by the ratios of cracked beam natural frequencies to the uncracked beam natural frequencies (Swamidas et al. 2004; Owolabi et al. 2003; Nahvi and Jabbari 2005). In this last case, the knowledge of the material properties (the Young's modulus E and the density ρ) are not required, but the natural frequencies of the uncracked beam are needed.
In this paper, an alternative criterion will be presented in order to avoid a careful determination of the material properties or the knowledge of the uncracked frequencies of the beam. Even if the estimation of material properties may be easily investigated, the criterion that will be developed in the next section has the advantage to save experimental time and to obtain a robust damage identification.
Moreover, these methodology will be extended by considering not only the identification of the crack size and location but also the orientation of the crack χ, as indicated in Figure 1.
The proposed criterion is based on the two following facts :

- the changes in the ratios of two natural frequencies is not affected by the material properties (i.e. the Young modulus E and the density ρ),
- the natural frequencies associated with the vertical (first, third and fifth frequencies) and horizontal (second, fourth, and sixth frequencies) modes are equal in the case of an uncracked beam, but are different for the cracked beam due to the size, position and orientation of the crack (as illustrated in Figures 2, 3 and 4).

Therefore, the proposed criterion is based on the ratio changes of the natural frequency of the vertical and horizontal modes of the cracked beam

$$\%\Delta_i^{cracked}(\mu,\chi,L_{crack}) = 100\times\frac{\omega_{2i-1}^{cracked}(\mu,\chi,L_{crack})-\omega_{2i}^{cracked}(\mu,\chi,L_{crack})}{\omega_{2i-1}^{cracked}(\mu,\chi,L_{crack})} \quad (15)$$

where $\omega_{2i-1}^{cracked}$ and $\omega_{2i}^{cracked}$ correspond to the natural frequency of the i^{th} vertical and horizontal modes, respectively. The evolutions of $\%\Delta_i^{cracked}$ (for $i = 1,\ldots,3$) are shown in Figures 5: it may be observed that this criterion $\%\Delta_i^{cracked}$ is dependent on the non-dimensional crack depth μ, the crack location L_{crack} and the crack orientation χ, and is obtained by only considering the cracked natural frequencies of the beam. Here, it is assumed that the open crack area remains constant which allows the determination of $\Delta_i^{cracked}$.

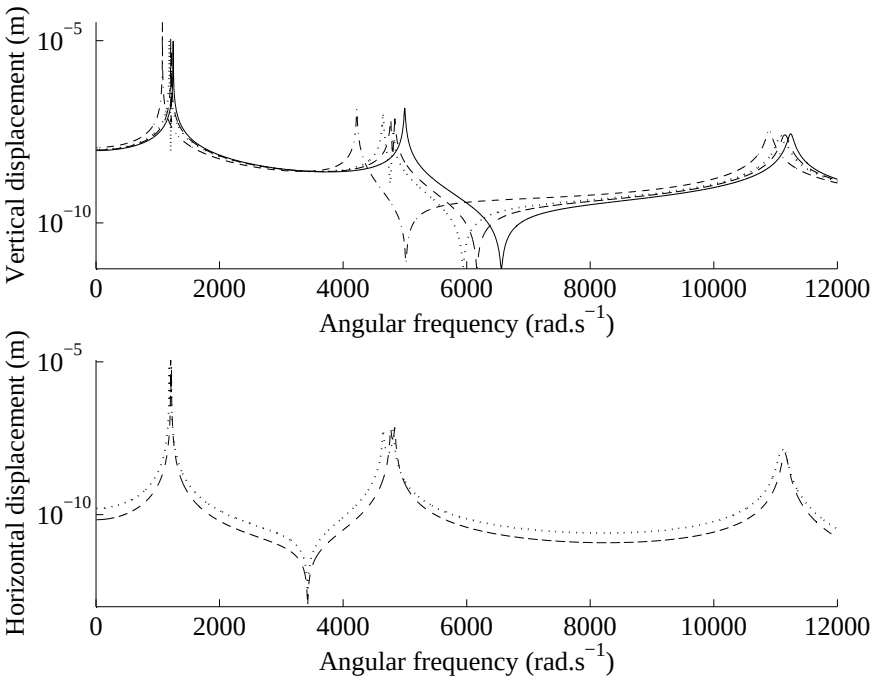

Figure 2 : Evolution of the absolute vertical and horizontal responses as a function of the crack front orientation for $\mu = 1$ and $L_{crack} = 0.716m$ (uncracked $-$; cracked with $\cdots$ $\chi = \frac{\pi}{3} rad.$, $--$ $\chi = \frac{\pi}{2} rad.$, $-.-$ $\chi = 0\,rad.$)

In order to illustrate the Frequencies' Ratio Surfaces Intersection method , a crack is added on the beam: the value of the non-dimensional crack depth is $\mu = 0.8$, the crack orientation is $\chi = \frac{\pi}{3} rad.$ and the crack is located at $L_{crack} = 0.15m$ (see case 1 in Table 2). Then, Table 3 gives the values of $\%\Delta_i^{cracked}$ (with $i = 1,\ldots,3$) for this assumed crack. Figures 6 illustrate the combinations of different crack locations, crack depths and crack orientations which have the same ratio changes $\%\Delta_i^{cracked}(\mu,\chi,L_{crack})$ (for $i = 1,\ldots,3$). Each combination may be plotted as a surface with crack location L_{crack}, crack depth μ, and crack orientation χ as its axes. Then, the intersections of the three surfaces of the first three percentage ratio changes $\%\Delta_i^{cracked}(\mu,\chi,L_{crack})$ define the different possible combinations of crack locations, crack depths and crack orientations for the cracked beam under study. It clearly appears that the intersections of the three surfaces defines two similar contour lines indicating two values for the crack location L_{crack} and couples of values (μ,χ) for the crack size μ and the crack orientation χ. These two intersections of the three surfaces are indicated by the red lines in Figures 6. It is well known that the non-uniqueness of the damage location L_{crack} is only due to structural symmetry of the beam (Dilena and Morassi 2004; Swamidas et al. 2004).

Then, due to the fact that it is assumed that the portion of the crack lying below the neutral axis is opened under the effect of self weight bending, the area of the open crack may correspond to various orientations of the crack front χ and non-dimensional crack depths μ. The two lines that correspond to the intersection of the three surfaces, define all the possible couples of values (μ,χ) for the cracked beam under study. As required for the frequency contour lines method (Swamidas et al. 2004; Owolabi et al. 2003; Nahvi and Jabbari 2005), a minimum of three ratio frequency surfaces $\%\Delta_i^{cracked}$ is required. Effectively, if the crack is situated at the node of the i^{th} vertical and horizontal modes, $\omega_{2i-1}^{cracked}$ and $\omega_{2i}^{cracked}$ remain almost unchanged. Thereby, the associated ratio change $\Delta_i^{cracked}$ is equal to zero and the identification is not possible.

In conclusion, the Frequencies' Ratio Surfaces Intersection method is based on a new criterion $\%\Delta_i^{cracked}$ that only considers the natural frequencies of the cracked beam. The natural frequencies of the uncracked beam are not used, and an accurate knowledge of the material properties (i.e. the Young's modulus E and the density ρ) is not needed.

The process considers the surfaces which have the same ratio changes $\%\Delta_i^{cracked}$ resulting in a combination of dif-

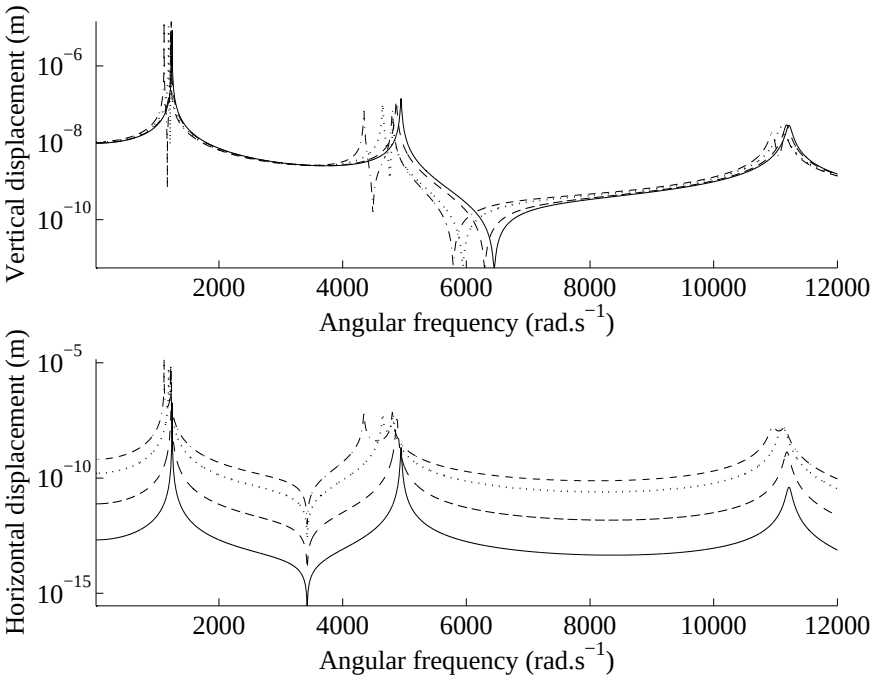

Figure 3 : Evolution of the absolute vertical and horizontal responses as a function of the non-dimensional crack depth μ for $\chi = \frac{\pi}{3} rad.$ and $L_{crack} = 0.716m$($-$ $\mu = 0.25$, $--$ $\mu = 0.5$, $\cdots$ $\mu = 1$, $-.-$ $\mu = 1.5$)

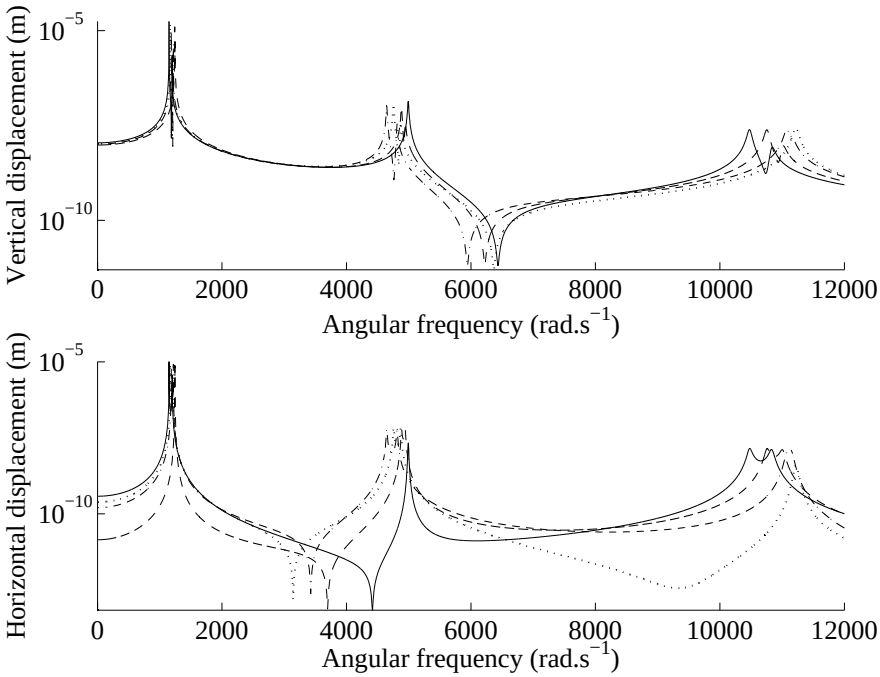

Figure 4 : Evolution of the absolute vertical and horizontal responses as a function of the crack position L_{crack} $\chi = \frac{\pi}{3} rad.$ and $\mu = 1$ ($-$ $L_{crack} = 0.483m$, $--$ $L_{crack} = 0.916m$, $\cdots$ $L_{crack} = 0.65m$, $-.-$ $L_{crack} = 0.716m$)

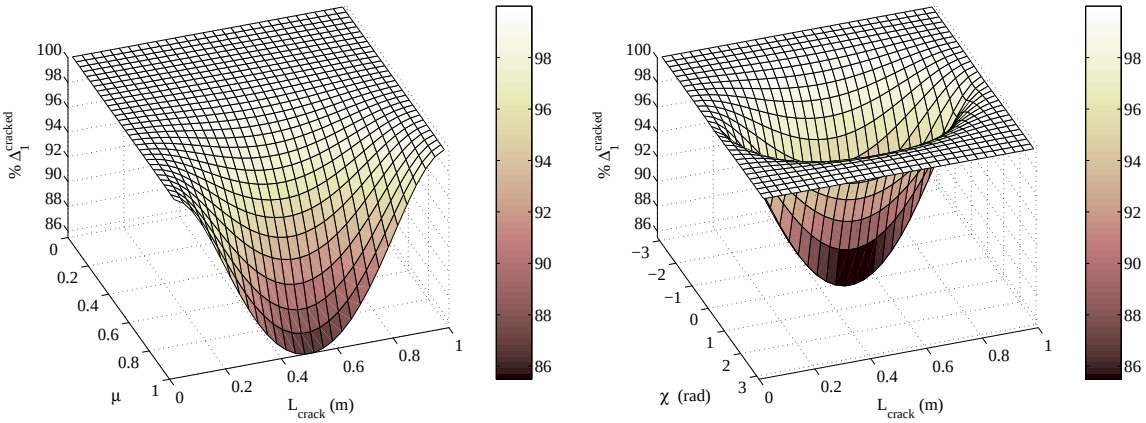

(a) $\%\Delta_1^{cracked}$ for $\chi = 0\,rad$. (b) $\%\Delta_1^{cracked}$ for $\mu = 1$

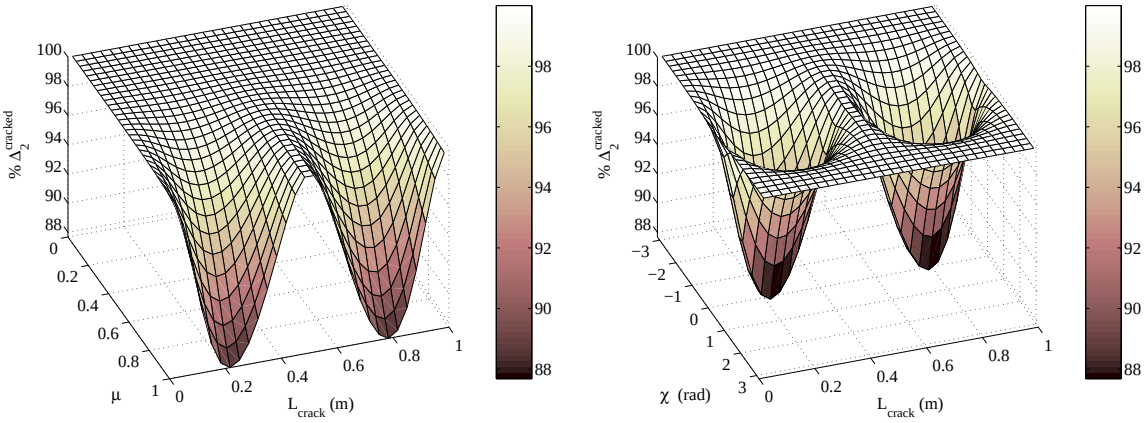

(c) $\%\Delta_2^{cracked}$ for $\chi = 0\,rad$. (d) $\%\Delta_2^{cracked}$ for $\mu = 1$

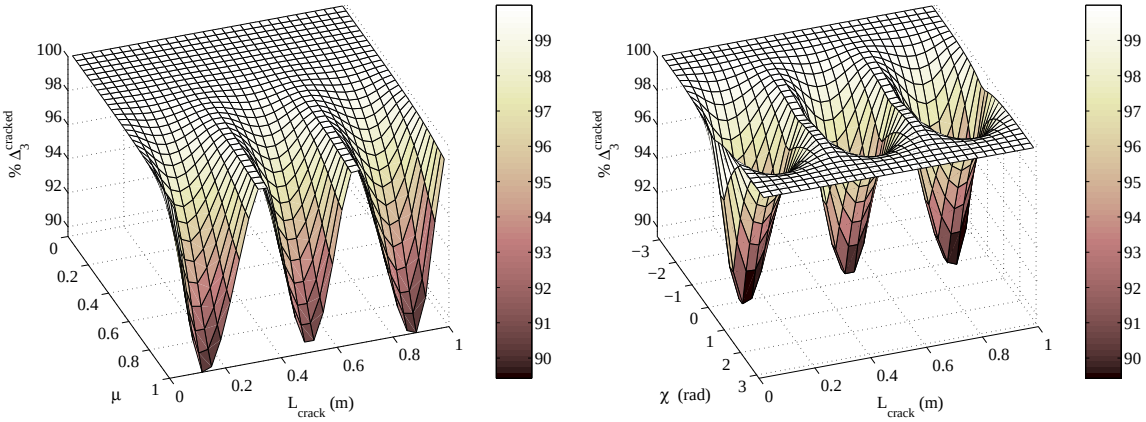

(e) $\%\Delta_3^{cracked}$ for $\chi = 0\,rad$. (f) $\%\Delta_3^{cracked}$ for $\mu = 1$

Figure 5 : Evolution of $\%\Delta_i^{cracked}$

ferent crack locations, crack depths and crack orientations can be plotted as a curve with crack location and crack depth as its axes. Then, the intersections of the surfaces $\%\Delta_i^{cracked}(\mu,\chi,L_{crack})$ for the three lower modes (for $i=1,\ldots,3$) indicates all the possible combinations of the crack position, the crack size and the crack orientation.

3.2 Non-uniqueness of the damage location based on antiresonances

As indicated in Figures 6, the identification procedure presented in the previous section is not sufficient to eliminate symmetrical solutions in the damage location problem. Effectively, it is well known that a crack at any end of the simply supported beam produces identical shifts in natural frequencies, and identical changes in the criterion $\Delta_i^{cracked}$.

In order to avoid the non-uniqueness of the damage location problem, some researchers (Swamidas et al. 2004; Sinou 2007) proposed to add an off-center placed mass to the simply supported beam from the left or right end. Due to this added off-center mass, the previous symmetry of the uncracked supported beam does not exist and the crack location may be identified. However, it was demonstrated that this methodology may be difficult to be used (see for example (Sinou 2007)).

Recently, Dilena and Morassi (Dilena and Morassi 2004) proposed an appropriate use of resonances and antiresonances in order to avoid the non-uniqueness of the damage location problem due to structural symmetry. One of the advantages of using antiresonances is that no additional tests is necessary, contrary to the previous methodology. Moreover, it should be noted that antiresonances like resonances are easily measurable.

As previously explained in Section 2.3, the presence of cracks may induced coupling of the two lateral vibrations if the crack is fully or partially open and if the crack front is different from the direction of the external force that is assumed to be directed on the vertical X-axis. It may be noted that no displacement will be observed in the horizontal direction if the system is uncracked due to the fact that the excitation is only in the vertical direction.

Then, as explained by Wahl et al. (Wahl et al. 1996), the resonances and antiresonances alternate continuously only for the Frequency Response Function of the driving point where the response co-ordinate and the excitation co-ordinate are identical. Moreover, by increasing the distance between the excitation co-ordinate and the response co-ordinate, the number of antiresonance ranges decreases. Considering Equations 9 and 14, the presence of a transverse crack introduces an excitation force at the crack location in the horizontal and vertical directions. So, if the external force is only directed on the vertical axis (and the crack front is different from the direction of the external force), the Frequency Response Functions of the horizontal degrees-of-freedom appear only due to the crack force's excitation. Thereby, the response co-ordinate where the resonances and antiresonances alternate continuously defines the vicinity of the crack location. Figures 7 illustrate the Frequency Response Functions for all the horizontal degrees-of-freedom of the cracked beam (at several locations along the shaft named by "shaft"-axis in the figures) when the sinusoidal external excitation is situated at the left end (see Figure 7 (a)) or the right end (see Figure 7 (b)) of the simply supported beam. It is clearly shown that the non-uniqueness location of the crack may be avoid by using antiresonances. If the external force and the crack location are close, it may be observed that resonances and antiresonances can alternate for all the degrees-of-freedom of the beam (see Figure 7 (a)). However, considering Figure 7 (b), it clearly appears that the resonances and antiresonances alternate continuously only at one end of the beam. So the non-uniqueness of the damage location may be avoid by only considering the Frequency Response Functions and the use of the driving point FRF that is characterized by a successive change in the resonances and antiresonances.

3.3 Identification of the crack depth and crack orientation

As previously explained, the two contour lines that corresponds to the intersection of the three surfaces having the same ratio changes $\%\Delta_i^{cracked}$ (for $i=1,\ldots,3$), result in a combination of different crack locations, crack depths and crack orientations. The damage location being obtained by using the antiresonances, only the size and orientation of the crack need to be determined. So, the contour line of Figures 6 illustrates all the combinations of the non-dimensional crack size μ and the crack orientations χ that correspond to the equivalent open crack (i.e. the portion of the crack lying below the neutral axis under the effect of self weight bending).

By rotating the beam by chosen angles, the portion of the crack lying below the neutral axis changes. So the

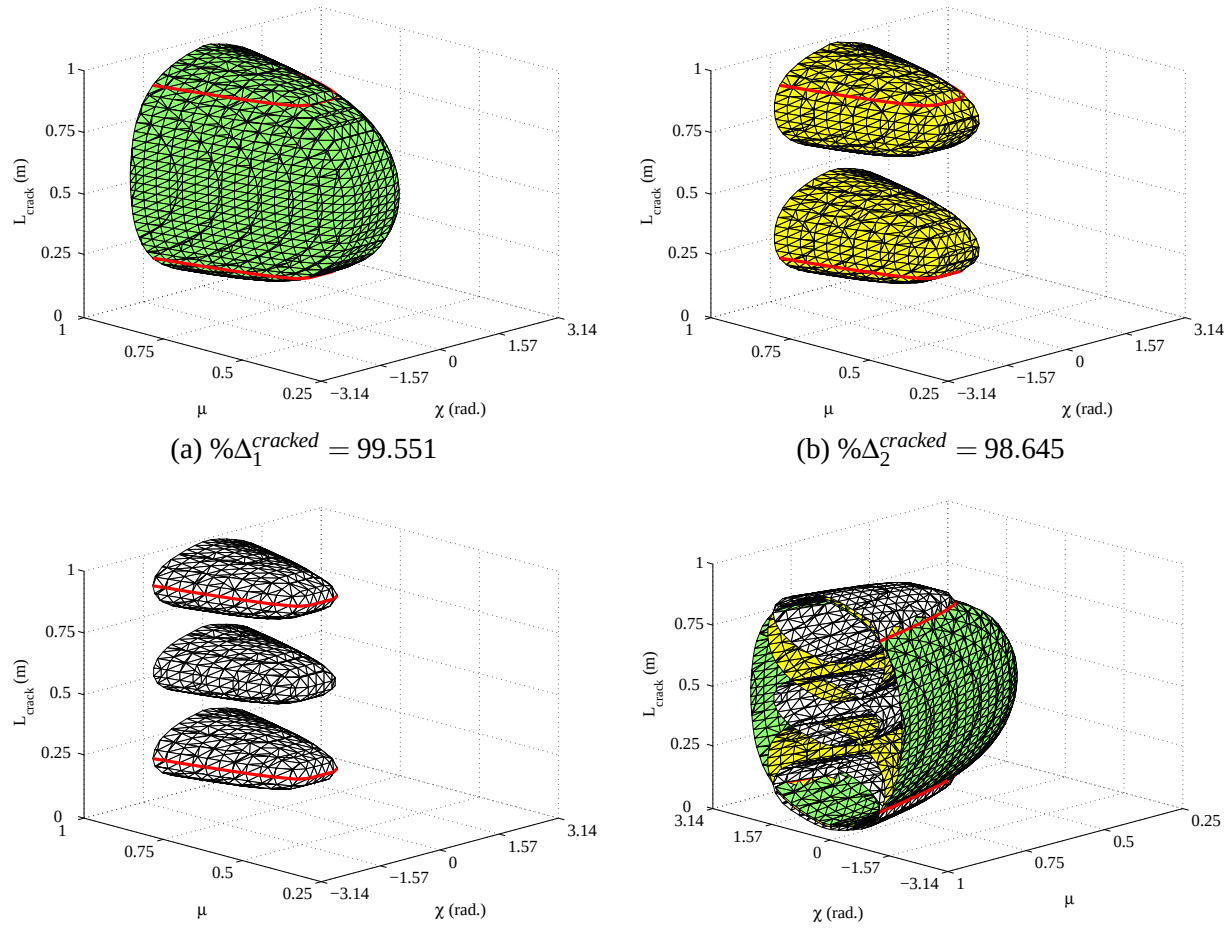

(a) $\%\Delta_1^{cracked} = 99.551$ (b) $\%\Delta_2^{cracked} = 98.645$

(c) $\%\Delta_3^{cracked} = 98.279$ (d) Intersections of the three surfaces

Figure 6 : Surfaces $\%\Delta_1^{cracked}$, $\%\Delta_2^{cracked}$ and $\%\Delta_3^{cracked}$ and intersections of the three surfaces (red lines) for $\mu = 0.8$, $\chi = \frac{\pi}{3}$ and $L_{crack} = 0.15m$

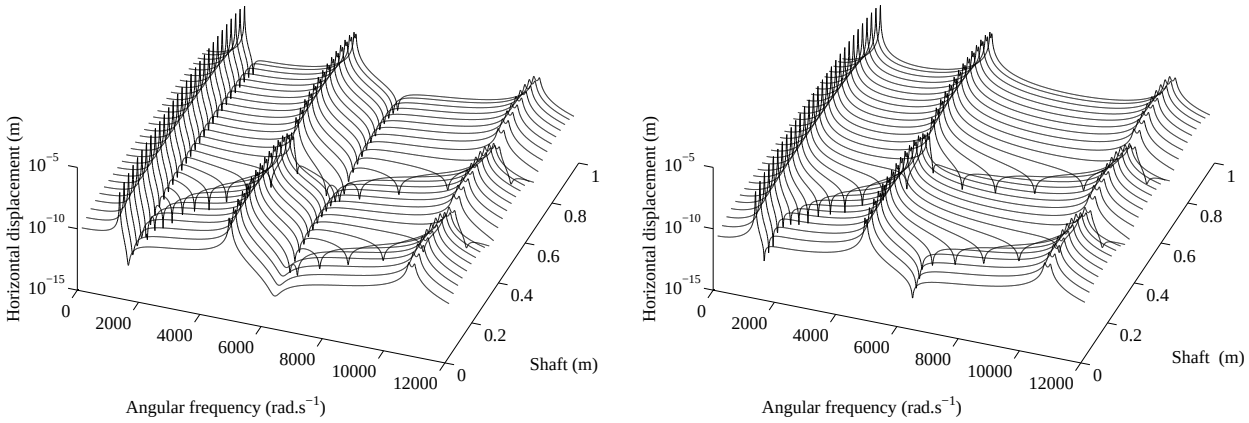

(a) Excitation at $0.16m$ (b) Excitation at $0.84m$

Figure 7 : Identification on the non-uniqueness of the crack location based on the vertical displacements of the crack beam

Table 2 : Values of the crack depth, crack location and crack orientation for the five cases under study

Case	Non-dimensional crack depth μ	Crack location L_{crack} (m)	Crack orientation χ (rad.)
1	0.8	0.15	$\frac{\pi}{3}$
2	0.3	0.62	$\frac{\pi}{5}$
3	0.5	0.28	$\frac{2\pi}{3}$
4	0.7	0.48	$\frac{\pi}{2}$
5	0.9	0.42	$\frac{\pi}{10}$

Table 3 : Values of $\%\Delta_i^{cracked}$

μ	$L_{crack}(m)$	$\chi(rad.)$	Angle (rad.)	open crack area (mm^2)	$\%\Delta_1^{cracked}$	$\%\Delta_2^{cracked}$	$\%\Delta_3^{cracked}$
0.8	0.15	$\frac{\pi}{3}$	χ	2092	99.551	98.645	98.279
			$\chi+\pi/2$	2689	98.934	96.864	96.258
			$\chi+\pi$	841	99.977	99.928	99.899
			$\chi-\pi/2$	244	99.999	99.998	99.998
0.3	0.62	$\frac{\pi}{5}$	χ	739	99.936	99.968	99.985
			$\chi+\pi/2$	710	99.944	99.972	99.987
			$\chi+\pi$	0	100	100	100
			$\chi-\pi/2$	29	100	100	100
0.5	0.28	$\frac{2\pi}{3}$	χ	294	99.997	99.996	99.999
			$\chi+\pi/2$	1535	99.544	99.352	99.866
			$\chi+\pi$	1242	99.77	99.666	99.93
			$\chi-\pi/2$	0	100	100	100
0.7	0.48	$\frac{\pi}{2}$	χ	1225	99.646	99.995	99.684
			$\chi+\pi/2$	2450	96.686	99.952	97.311
			$\chi+\pi$	1225	99.646	99.995	99.684
			$\chi-\pi/2$	0	100	100	100
0.9	0.42	$\frac{\pi}{10}$	χ	3246	91.937	98.104	96.475
			$\chi+\pi/2$	2103	98.104	99.529	99.094
			$\chi+\pi$	182	99.999	100	99.999
			$\chi-\pi/2$	1325	99.573	99.891	99.786

combinations of the crack size μ and the crack orientation χ that corresponds to the new equivalent open crack also change. Figure 8 illustrates the different contour lines that may be obtained for various chosen rotations of cracked beam. In our cases, three successive angle rotations ($-\frac{\pi}{2}$, $\frac{\pi}{2}$ and π) have been chosen. It may be noted that all these lines define the combination of the crack orientations and crack sizes for a given orientation of the crack beam. So, knowing the angle variation between two contour lines (i.e. the angle rotation that has been chosen), the uniqueness of the crack orientation and crack size may be determined graphically, as indicated in Figure 8: effectively, all the combinations of different crack orientations and crack depths can be plotted as a curve with crack orientation and crack depth as its axes. The intersection of the contour lines indicates the non-dimensional crack depth μ and the crack orientation χ (in regard to the first initial orientation of the cracked beam). It may be noted that the identification of the non-dimensional crack depth and crack orientation can be defined by the intersection of two, three or four contour lines due to the fact that the transverse crack may be totally closed for some orientations of the cracked beam and partially opened for the others, as indicated in table 3.

Finally, it may be observed that the point that corresponds to the intersections of the different contour lines may be defined as the intersection of all the surfaces

$\%\Delta_1^{cracked}$, $\%\Delta_2^{cracked}$ and $\%\Delta_3^{cracked}$ for the various chosen rotations of cracked beam.

In conclusion, the crack size, crack orientation and crack location have been identified. The proposed method, called the Frequencies' Ratio Surfaces Intersection method (FRSI-method), only considers the natural frequencies of the cracked beams and does not require an accurate knowledge of the material properties (i.e. the Young's modulus E and the density ρ).

3.4 Numerical validation

In order to numerically demonstrate the efficiency of the proposed methodology in the case of a simply supported beam with various crack locations, depths and orientations, four additional cases will be undertaken, as indicated in Table 2. The intersections of the three surfaces of $\%\Delta_i^{cracked}(\mu,\chi,L_{crack})$ (for $i=1,\ldots,3$) are given in Figures 9 for the four last cases. Table 3 indicates the values of the associated factors $\%\Delta_i^{cracked}$. It may be observed that theses intersections are double for each case. So, using the Frequency Response Functions and antiresonances enable us to identify the crack location, as illustrated in Figures 10. It may be observed that the use of antiresonances is possible even if the equivalent area of the open crack is small (due to the combination of the crack orientation and crack depth, as indicated in Table 3).

Finally, the identification of the non-dimensional crack depth and the crack orientation is obtained by rotating the beam by three angles ($-\frac{\pi}{2}$, $\frac{\pi}{2}$ and π). The intersections of the contour lines that indicate the crack depth and crack orientation are shown for the four cases in Figures 11. In conclusion, the crack depth, crack location and crack orientation are identified in all cases.

4 Extension of the FRSI-method and robust identification

4.1 Extension of the Frequencies' Ratio Surfaces Intersection method

The previous RFSI-method may be extended by considering the ratio of the i^{th} and j^{th} natural frequencies. In this case, the previous criterion $\%\Delta_i^{cracked}$ may be generalized by considering the new factor

$$\%\Psi_{i,j}^{cracked}(\mu,\chi,L_{crack}) = 100\times\left(\frac{\omega_i^{uncracked}}{\omega_j^{uncracked}}-\frac{\omega_i^{cracked}(\mu,\chi,L_{crack})}{\omega_j^{cracked}(\mu,\chi,L_{crack})}\right) \quad (16)$$

where $\omega_i^{uncracked}$ and $\omega_i^{cracked}$ correspond to the i^{th} natural frequencies of the uncracked and cracked simply supported beams, respectively.

It may be observed that the factor $\%\Delta_i^{cracked}$ corresponds to the expression 16 where $\frac{\omega_i^{uncracked}}{\omega_j^{uncracked}}$ is equal to one that defines an uncracked symmetrical beam. Effectively, we have

$$\begin{aligned}\%\Delta_i^{cracked} &= 100\times\frac{\omega_{2i-1}^{cracked}-\omega_{2i}^{cracked}}{\omega_{2i-1}^{cracked}}\\ &= 100\times\left(1-\frac{\omega_{2i}^{cracked}}{\omega_{2i-1}^{cracked}}\right)=\%\Psi_{2i,2i-1}^{cracked}\end{aligned} \quad (17)$$

Considering the case of a simply supported uncracked beam with a circular cross section, the classical expression of the n^{th} natural frequency is given by (Harris and Piersol 2002)

$$\omega_n^{uncracked} = n^2\pi^2\sqrt{\frac{EI}{\rho SL^4}}=\frac{n^2\pi^2R}{2L^2}\sqrt{\frac{E}{\rho}} \quad (18)$$

where n are the modes numbers ($n=1,2,\ldots$). L and R are the length and the radius of the uncracked beam. E and ρ define the Young's modulus and density, and so correspond to the material properties. I and S are the moment of inertia and area of the beam section.

Due to the symmetrical properties of the uncracked beam, it may be observed that the factor $\%\Psi_{i,j}^{cracked}(\mu,\chi,L_{crack})$ for the i^{th} and j^{th} pulsations can be rewritten by

$$\%\Psi_{2\alpha-a,2\beta-b}^{cracked}(\mu,\chi,L_{crack}) = 100\times\left(\left(\frac{\alpha}{\beta}\right)^2-\frac{\omega_{2\alpha-a}^{cracked}(\mu,\chi,L_{crack})}{\omega_{2\beta-b}^{cracked}(\mu,\chi,L_{crack})}\right) \quad (19)$$

with a and b are equal to 0 or 1, and $\alpha\in\aleph^*$ and $\beta\in\aleph^*$. If the numbers i and j are odd numbers (respectively even numbers), the factor $\%\Psi_{i,j}^{cracked}$ defines the ratio of the i^{th} and j^{th} natural frequencies that are only

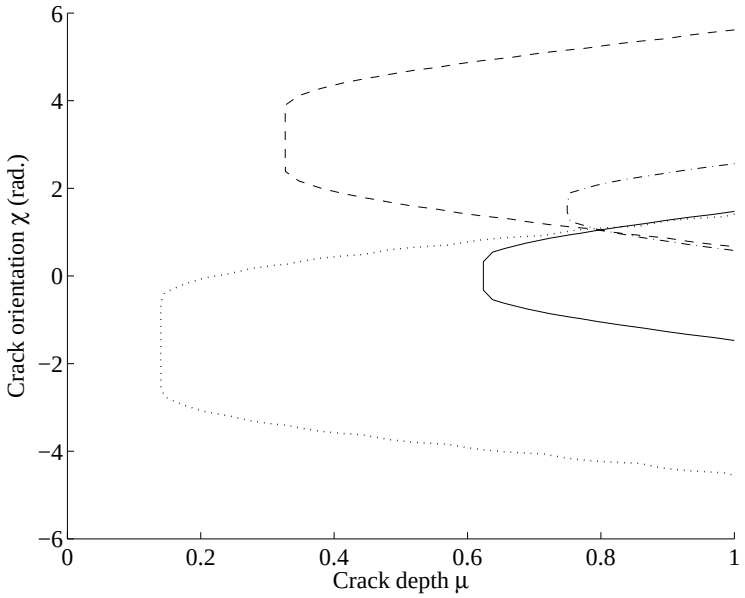

Figure 8 : Identification of the crack size μ and the crack orientation χ ($-\chi$, $-.-\chi+\frac{\pi}{2}rad.$, $--\chi+\pi rad.$, $\cdots\chi-\frac{\pi}{2}rad.$)

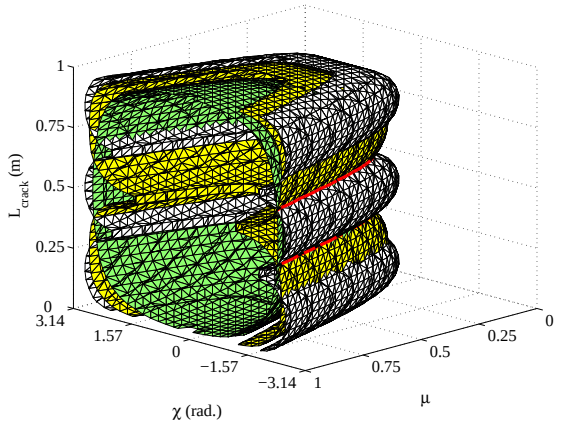

(a) $\mu=0.3$, $\chi=\frac{\pi}{5}rad.$, $L_{crack}=0.62m$

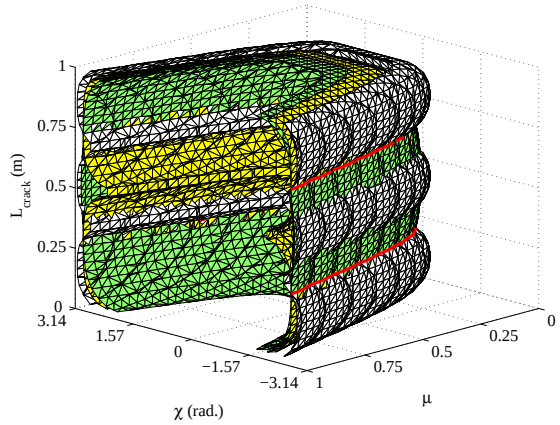

(b) $\mu=0.5$, $\chi=\frac{2\pi}{3}rad.$, $L_{crack}=0.28m$

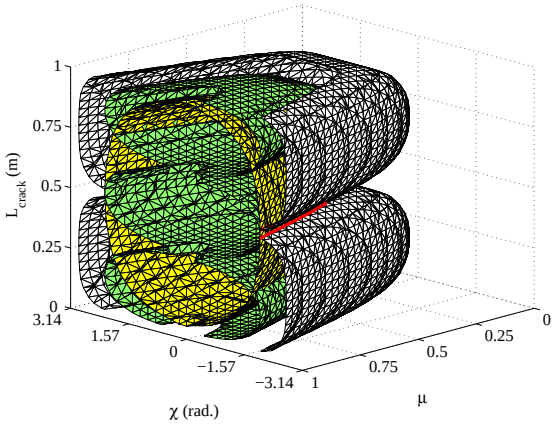

(c) $\mu=0.7$, $\chi=\frac{\pi}{2}rad.$, $L_{crack}=0.48m$

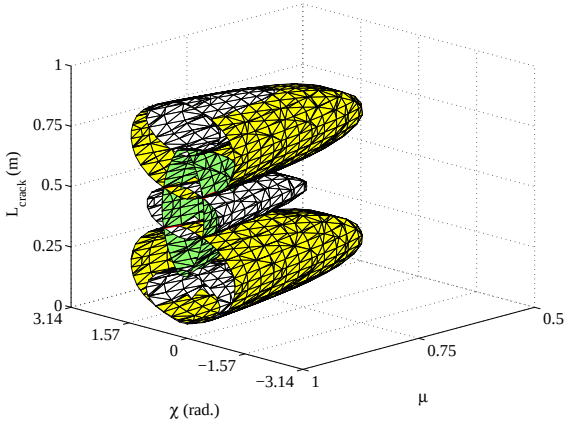

(d) $\mu=0.9$, $\chi=\frac{\pi}{10}rad.$, $L_{crack}=0.42m$

Figure 9 : Surfaces $\%\Delta_i^{cracked}$ (green=$\%\Delta_1^{cracked}$,yellow=$\%\Delta_2^{cracked}$, white=$\%\Delta_3^{cracked}$; red lines= surfaces' intersections)

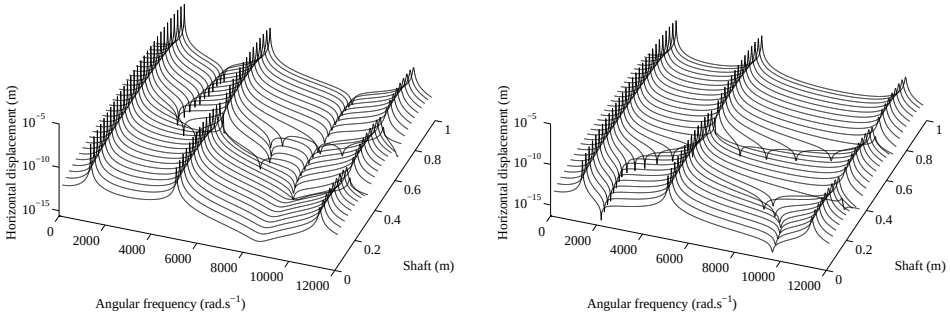

(a) $\mu = 0.3$, $\chi = \frac{\pi}{5} rad.$, $L_{crack} = 0.62m$ (b) $\mu = 0.5$, $\chi = \frac{2\pi}{3} rad.$, $L_{crack} = 0.28m$

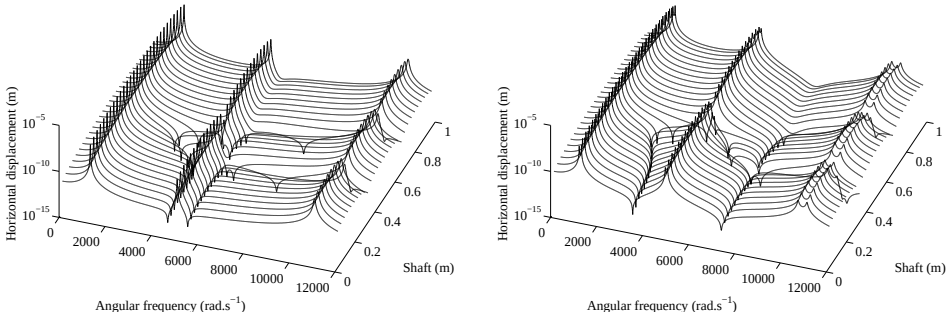

(c) $\mu = 0.7$, $\chi = \frac{\pi}{2} rad.$, $L_{crack} = 0.48m$ (d) $\mu = 0.9$, $\chi = \frac{\pi}{10} rad.$, $L_{crack} = 0.42m$

Figure 10 : Identification of the the crack location based on the vertical amplitudes and antiresonances

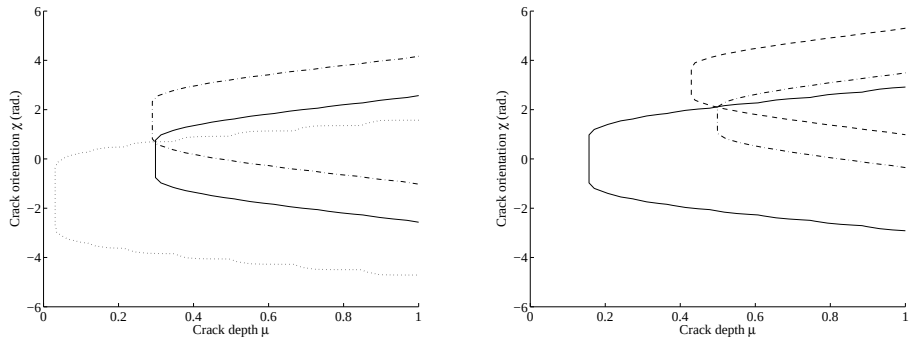

(a) $\mu = 0.3$, $\chi = \frac{\pi}{5} rad.$, $L_{crack} = 0.62m$ (b) $\mu = 0.5$, $\chi = \frac{2\pi}{3} rad.$, $L_{crack} = 0.28m$

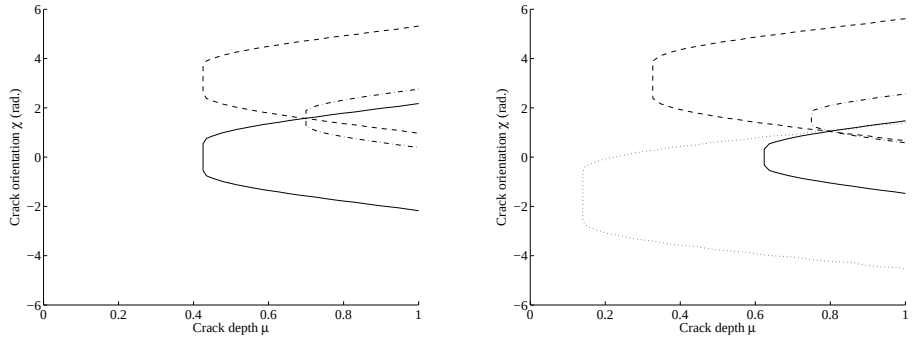

(c) $\mu = 0.7$, $\chi = \frac{\pi}{2} rad.$, $L_{crack} = 0.48m$ (d) $\mu = 0.9$, $\chi = \frac{\pi}{10} rad.$, $L_{crack} = 0.42m$

Figure 11 : Identification of the crack size μ and the crack orientation χ ($-\chi$, $-.-\chi + \frac{\pi}{2} rad.$, $--\chi + \pi rad.$, $\cdots \chi - \frac{\pi}{2} rad.$)

measured in one direction. If the number i is odd number (respectively even number) and the number j is even number (respectively odd number), the factor $\%\Psi_{i,j}^{cracked}$ defines the ratio of the i^{th} and j^{th} natural frequencies that are measured in horizontal (respectively vertical) and horizontal (respectively vertical) directions. Considering Equation 19, it is clear that the factors $\%\Psi_{i,j}^{cracked}$ are not only a function of crack depth, location and orientation, but also of the frequency number and the associated mode shape. Moreover, the factors $\%\Psi_{2\alpha-a,2\beta-b}^{cracked}$ need only the knowledge of the natural frequencies of the simply supported cracked beam and do not change with the variations of the material properties.

In order to illustrate the role of the factor $\%\Psi_{i,j}^{cracked}$, Figures 12 show the variations of $\%\Psi_{3,1}^{cracked}$, $\%\Psi_{5,1}^{cracked}$ and $\%\Psi_{5,3}^{cracked}$ with the non-dimensional crack depth, the crack size and the crack orientation. From the results obtained in these figures, it may be concluded that the mode of i^{th} natural frequency is more affected by the crack than the mode of j^{th} natural frequency if $\%\Psi_{i,j}^{cracked}$ is higher than 0. And so, if $\%\Psi_{i,j}^{cracked}$ is lower than 0, the more affected mode corresponds to the j^{th} natural frequency.
Effectively, Figures 12(a) and (b) indicate that when the crack location is between [0 0.3] or [0.7 1] (for the non-dimensional crack depth $\mu = 1$ and the orientation of the crack $\chi = 0rad.$), the first natural frequency that corresponds to the first vertical mode is comparatively much less affected than the third natural frequency that corresponds to the second vertical mode. For a crack situated between [0.3 0.7], the scenario is reversed. The same observations may be done for the comparison of the third and fifth natural frequencies that are associated with the second and third vertical modes of the cracked beam: when the crack is located between [0.15 0.4] and [0.6 0.85] (for $\mu = 1$ and $\chi = 0rad.$), the third natural frequency is more affected than the fifth natural frequency of the cracked beam.
Considering Figure 12, it can be seen that the factor $\%\Psi_{i,j}^{cracked}$ and the local associated minima and maxima indicate the trends of changes of the bending moment and its effect on both the mode of j^{th} natural frequency and the mode of i^{th} natural frequency.
Then, the minimum of the factor $\%\Psi_{i,j}^{cracked}$ reflects the fact that the j^{th} natural frequency is almost unaffected for a crack whereas the mode of i^{th} natural frequency is greatly affected. See for example Figure 12 when the crack is situated at one node of mode shapes (i.e. the middle of the beam for the second vertical and horizontal modes, and one-third of one end of the beam for the third vertical and horizontal modes).

4.2 Numerical validation

So the damage detection technique that has been explained in Section 3 can be extended by considering the evolutions of the factors $\%\Psi_{i,j}^{cracked}(\mu,\chi,L_{crack})$. As required for the factors $\%\Delta_i^{cracked}(\mu,\chi,L_{crack})$, a minimum of three ratio frequency surfaces $\%\Psi_{i,j}^{cracked}(\mu,\chi,L_{crack})$ is needed. For example Figures 13 show the three surfaces of the factors $\%\Psi_{3,1}^{cracked}$, $\%\Psi_{5,1}^{cracked}$ and $\%\Psi_{5,3}^{cracked}$. These surfaces define all the combinations of the different crack location L_{crack}, crack depth μ and crack orientation χ which have the same ratio changes of the factors $\%\Psi_{3,1}^{cracked}$, $\%\Psi_{5,1}^{cracked}$ and $\%\Psi_{5,3}^{cracked}$ for the cracked beam under study. The values of the factors $\%\Psi_{3,1}^{cracked}$, $\%\Psi_{5,1}^{cracked}$ and $\%\Psi_{5,3}^{cracked}$ are given in Table 4. It clearly appears that the factors $\%\Psi_{i,j}^{cracked}$ increase rapidly with increasing of the non-dimensional crack depth μ. Therefore, the detection of lower crack detph appears to be easily done.
As previously indicated in Section 3, the intersections of the three surfaces define two similar contour lines indicating two values for the crack location L_{crack} and the combinations (μ,χ) of the crack size μ and the crack orientation χ.
These intersections of the three surfaces are given in Figures 13 by the red contour lines. It may be observed that only the first, second and third vertical modes (and the associated natural frequencies) of the cracked beam are used.
Then, the non-uniqueness of the crack location is avoid by considering the driving point Frequency Response Function that is characterized by a successive change in the resonances and antiresonances (see Section 3.2 and Figures 7). As indicated in Section 3.3, the non-dimensional crack depth μ and the crack orientation χ are determined graphically by rotating the beam by specified chosen angles, as illustrated in Figures 8. It may be observed that the combinations of the non-dimensional crack size μ and the crack orientation χ are the same for both the factors $\%\Delta_i^{cracked}(\mu,\chi,L_{crack})$ and $\%\Psi_{i,j}^{cracked}(\mu,\chi,L_{crack})$. Effectively, the area of the crack that is open is the same, so the calculated possible combinations (μ,χ) are equivalent.

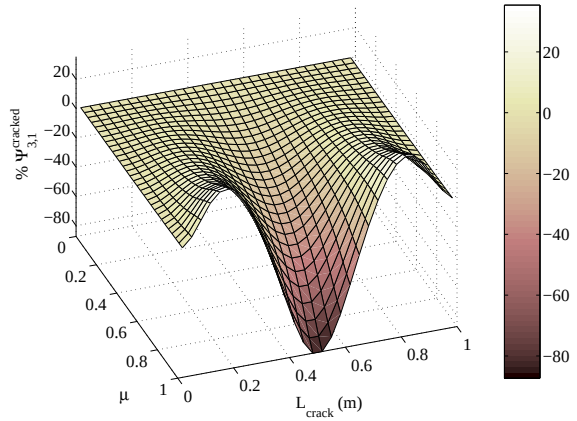

(a) $\%\Psi_{3,1}^{cracked}$ for $\chi = 0rad$.

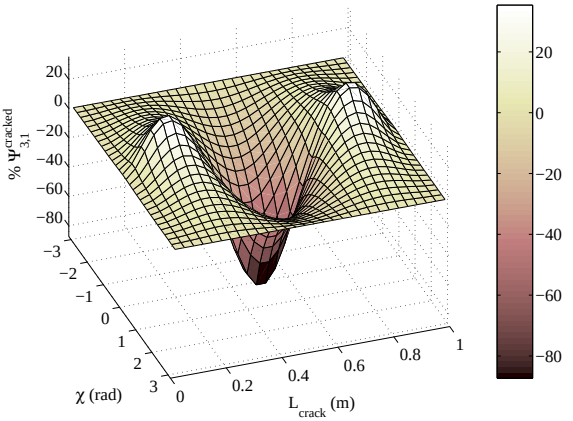

(b) $\%\Psi_{3,1}^{cracked}$ for $\mu = 1$

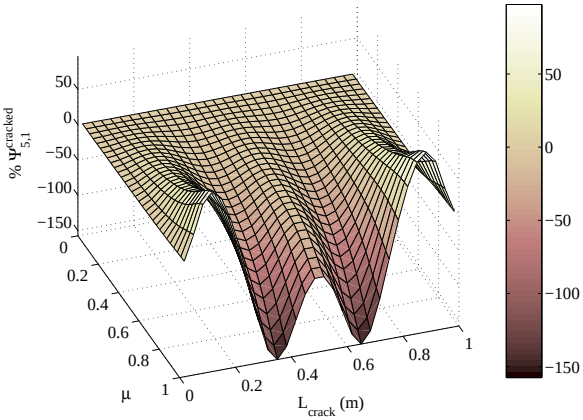

(c) $\%\Psi_{5,1}^{cracked}$ for $\chi = 0rad$.

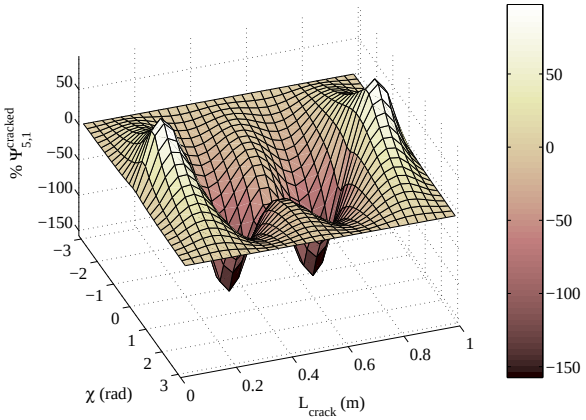

(d) $\%\Psi_{5,1}^{cracked}$ for $\mu = 1$

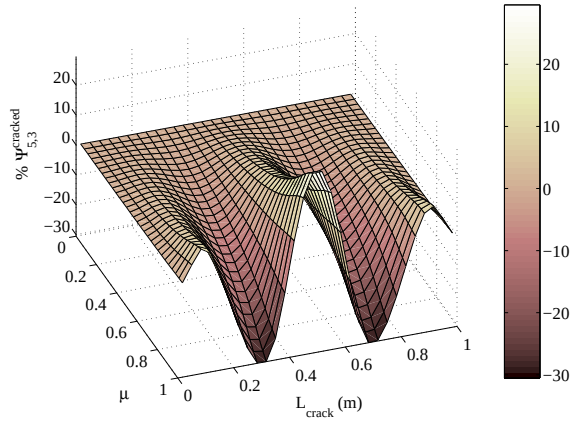

(e) $\%\Psi_{5,3}^{cracked}$ for $\chi = 0rad$.

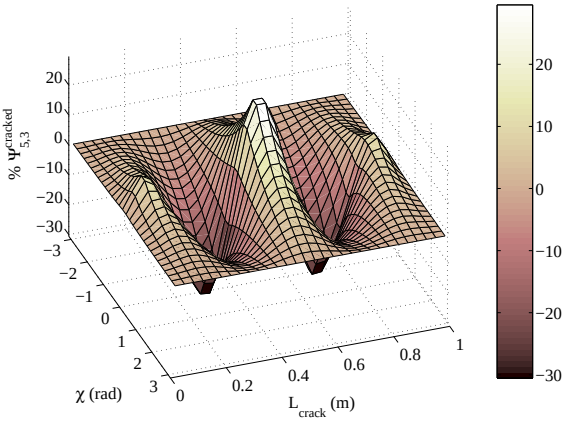

(f)$\%\Psi_{5,3}^{cracked}$ for $\mu = 1$

Figure 12 : Evolution of $\%\Psi_{i,j}^{cracked}$

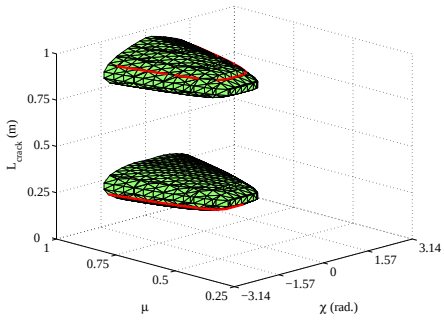

(a) $\%\Psi_{31}^{cracked}$

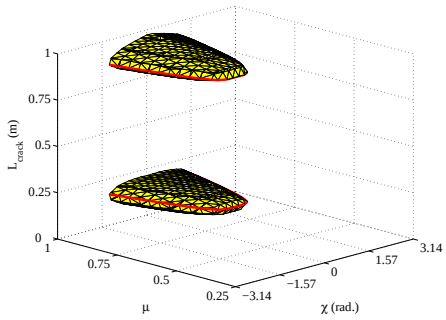

(b) $\%\Psi_{51}^{cracked}$

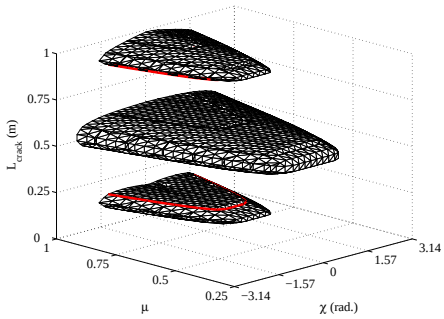

(c) $\%\Psi_{53}^{cracked}$

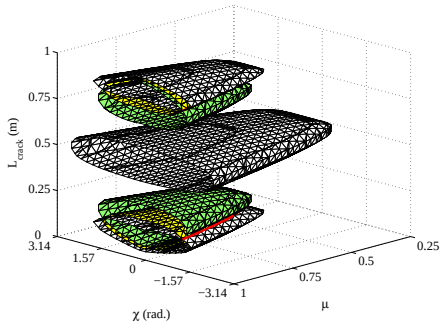

(d) Intersections of the three surfaces

Figure 13 : Surfaces $\%\Psi_{31}^{cracked}$, $\%\Psi_{51}^{cracked}$ and $\%\Psi_{53}^{cracked}$ (red lines= surfaces' intersections)

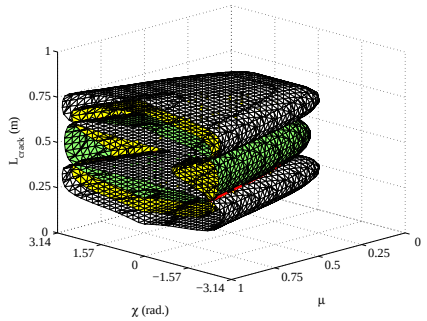

(a) $\mu = 0.3, \chi = \frac{\pi}{5} rad., L_{crack} = 0.62m$

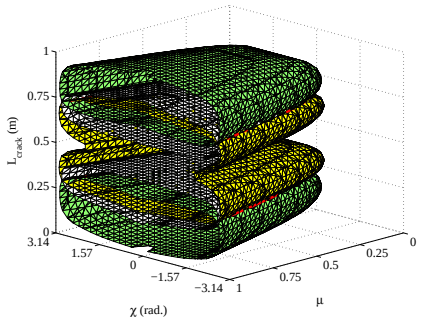

(b) $\mu = 0.5, \chi = \frac{2\pi}{3} rad., L_{crack} = 0.28m$

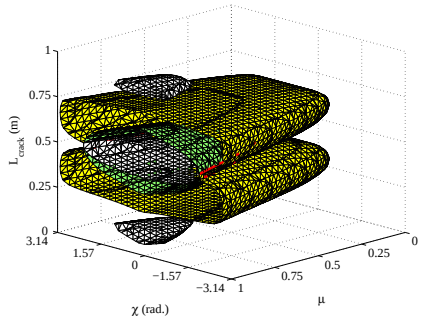

(c) $\mu = 0.7, \chi = \frac{\pi}{2} rad., L_{crack} = 0.48m$

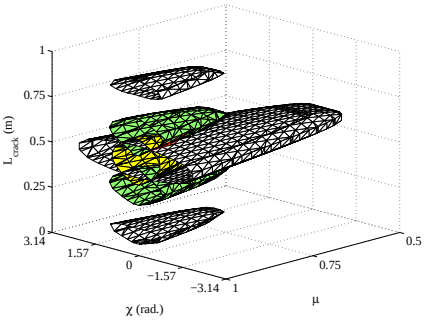

(d) $\mu = 0.9, \chi = \frac{\pi}{10} rad., L_{crack} = 0.42m$

Figure 14 : Surfaces $\%\Psi_{ij}^{cracked}$ (green=$\%\Psi_{31}^{cracked}$,yellow=$\%\Psi_{51}^{cracked}$, white=$\%\Psi_{53}^{cracked}$; red lines= surfaces' intersections)

Table 4 : Values of $\%\Psi_{ij}^{cracked}$

μ	$L_{crack}(m)$	$\chi(rad.)$	Angle (rad.)	$\%\Psi_{31}^{cracked}$	$\%\Psi_{51}^{cracked}$	$\%\Psi_{53}^{cracked}$
0.9	0.42	$\frac{\pi}{10}$	χ	-39.819	-63.4	5.955
			$\chi+\pi/2$	-16.334	-24.565	2.927
			$\chi+\pi$	-1.082	-1.554	0.22
			$\chi-\pi/2$	-8.623	-12.677	1.646
0.7	0.48	$\frac{\pi}{2}$	χ	-11.225	-1.815	5.7
			$\chi+\pi/2$	-30.088	-9.041	13.638
			$\chi+\pi$	-11.225	-1.815	5.7
			$\chi-\pi/2$	0	0	0
0.8	0.15	$\frac{\pi}{3}$	χ	10.192	34.67	3.011
			$\chi+\pi/2$	15.638	49.753	3.790
			$\chi+\pi$	3.323	12.262	1.206
			$\chi-\pi/2$	0.950	3.600	0.367
0.5	0.28	$\frac{2\pi}{3}$	χ	0.868	-2.283	-1.061
			$\chi+\pi/2$	4.445	-14.125	-6.099
			$\chi+\pi$	3.561	-10.737	-4.729
			$\chi-\pi/2$	0	0	0
0.3	0.62	$\frac{\pi}{5}$	χ	-2.811	-9.747	-0.85
			$\chi+\pi/2$	-2.692	-9.342	-0.815
			$\chi+\pi$	0	0	0
			$\chi-\pi/2$	-0.110	-0.390	-0.035

Finally, Figures 14 illustrate the surfaces' intersections of the factors $\%\Psi_{3,1}^{cracked}$, $\%\Psi_{5,1}^{cracked}$ and $\%\Psi_{5,3}^{cracked}$ for the four last cases that are given in Table 2. All the associated values of the factors $\%\Psi_{i,j}^{cracked}(\mu,\chi,L_{crack})$ are given in Table 4. In all cases, the crack location agrees with the previous identification done in Section 3.1.

In conclusion, it is shown that the identification of the crack parameters (location, depth and orientation) can be performed by considering the Frequencies' Ratio Surfaces Intersection method and the generalized factors $\%\Psi_{i,j}^{cracked}(\mu,\chi,L_{crack})$. The use of this generalized factor $\%\Psi_{i,j}^{cracked}$ allows to undertake an additionnal damage identification by verifying the previous identification for the crack location that has been obtained by using the factor $\%\Delta_i^{cracked}$. Moreover, these last factors may be usesul for the damage identification in structures where the natural frequencies are only measured in one direction (for example in rectangular cross section beams).

4.3 Sensibility of the FRSI-method and robust identification of the crack parameters

It is well known that experiments are frequently perturbed by noise measurement and that the proposed damage identification technique (Frequencies' Ratio Surfaces Intersection method) may be particularly sensitive to experimental and/or modeling errors. In this case, the identification of the crack location, size and orientation can be less or more difficultly obtained depending on the effect of uncertainties due to measurement errors and environmental conditions. So the robustness and sensibility of the Frequencies' Ratio Surfaces Intersection method through these hypotheses will be undertaken in this section with various noise levels for cases 1, 2 and 3.

In order to simulate correctly the presence of noise on measurements, several uniform random noises are added on the previous deterministic computational experiments (i.e. each frequency of the cracked system is modified by an uniformly distributed random noise level). Table 5 gives the values of the first sixth frequencies for cases 1, 2 and 3 without noise. Then, Tables 6, 7 and 8 show the evolutions of the frequencies for cases 1, 2 and 3 with

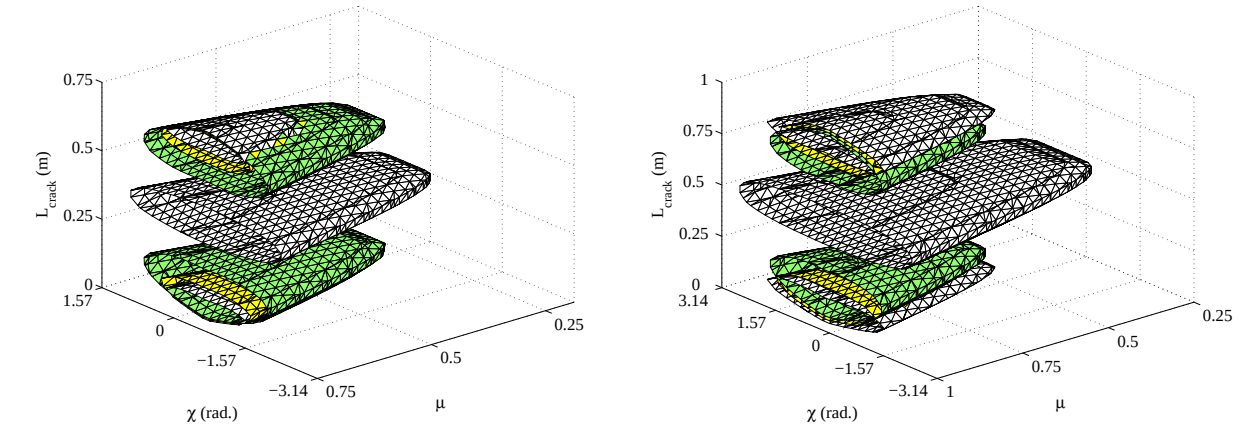

(a) 1% noise level (b) 2% noise level

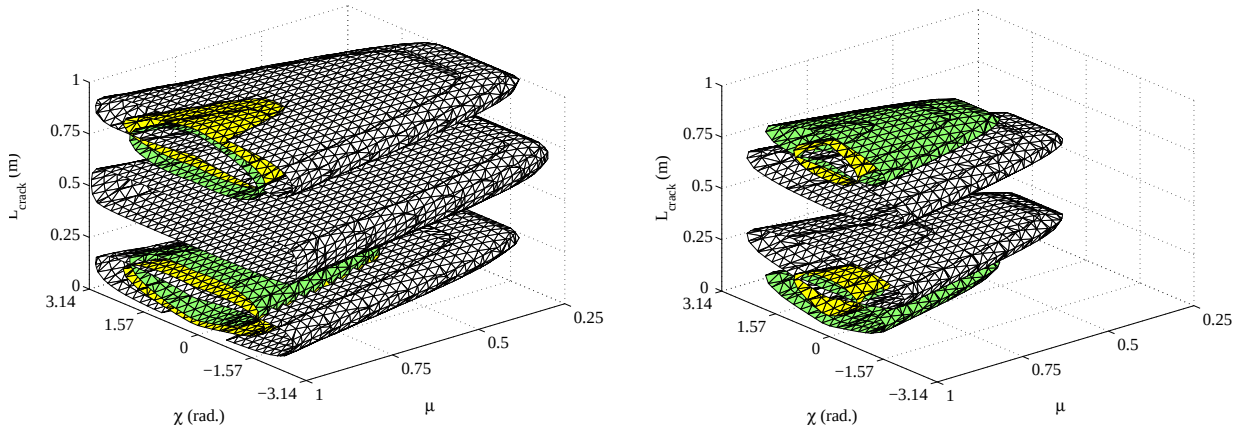

(c) 4% noise level (d) 6% noise level

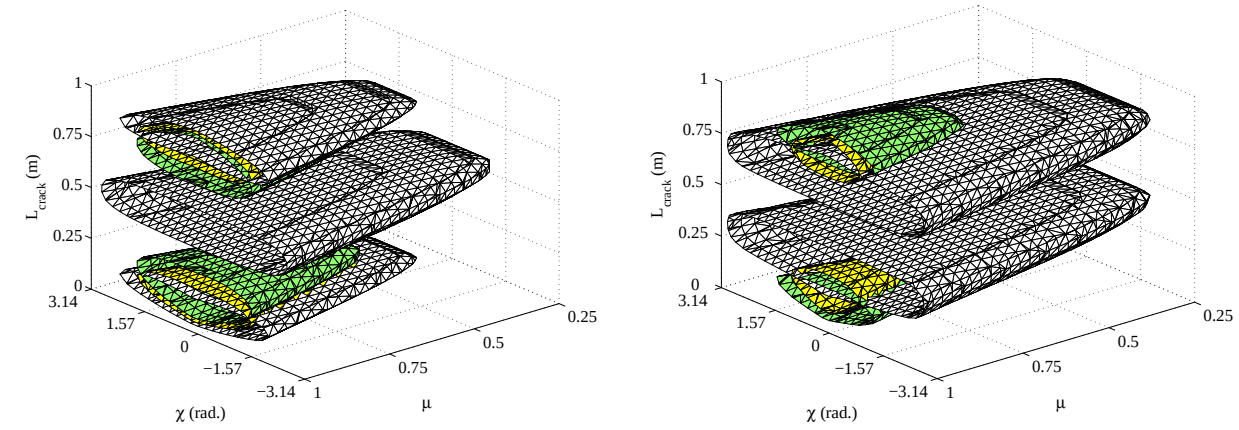

(e) 8% noise level (f) 10% noise level

Figure 15 : Surfaces $\%\Psi_{ij}^{cracked}$ with various noise levels for the case 1 ($\mu = 0.8$, $\chi = \frac{\pi}{3} rad.$ and $L_{crack} = 0.15m$, green=$\%\Psi_{31}^{cracked}$,yellow=$\%\Psi_{51}^{cracked}$, white=$\%\Psi_{53}^{cracked}$)

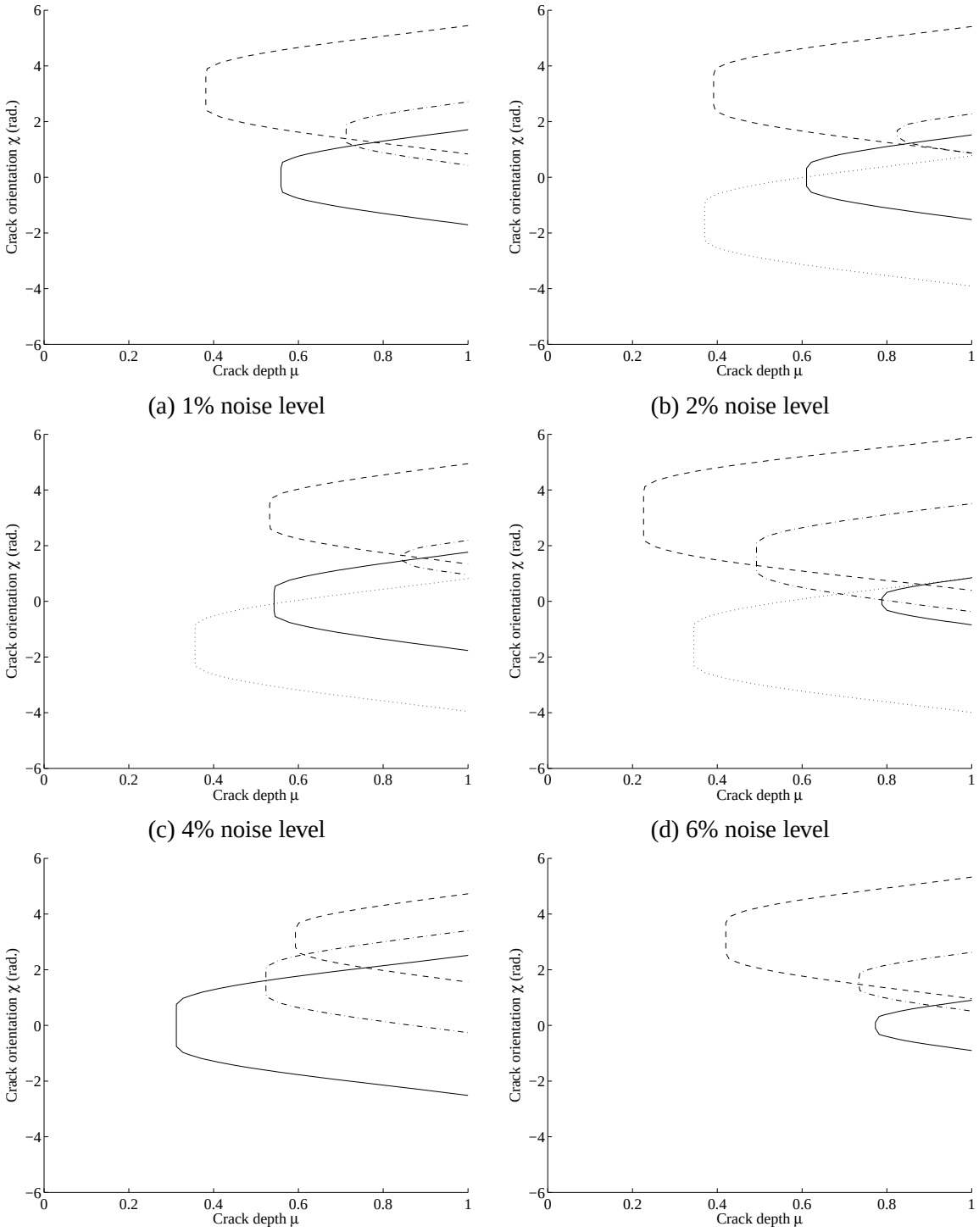

(a) 1% noise level

(b) 2% noise level

(c) 4% noise level

(d) 6% noise level

(e) 8% noise level

(f) 10% noise level

Figure 16 : Identification of the crack size μ and the crack orientation χ with various noise levels for the case 1 ($\mu = 0.8$, $\chi = \frac{\pi}{3} rad.$ and $L_{crack} = 0.15m$) and with the contour lines of $\Psi_{31}^{cracked}$ ($-\chi$, $-.-\chi + \frac{\pi}{2} rad.$, $--\chi + \pi rad.$, $\cdots \chi - \frac{\pi}{2} rad.$)

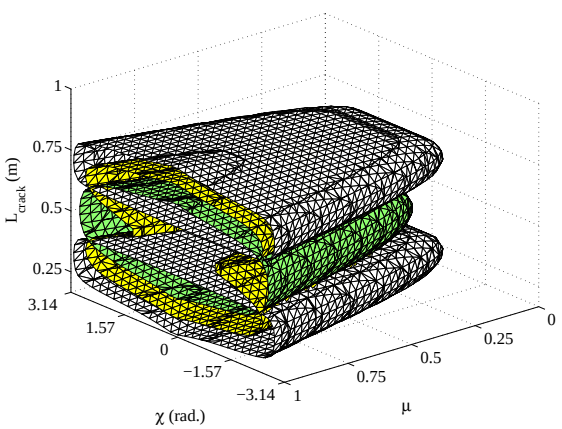

(a) Case 2, 1% noise level

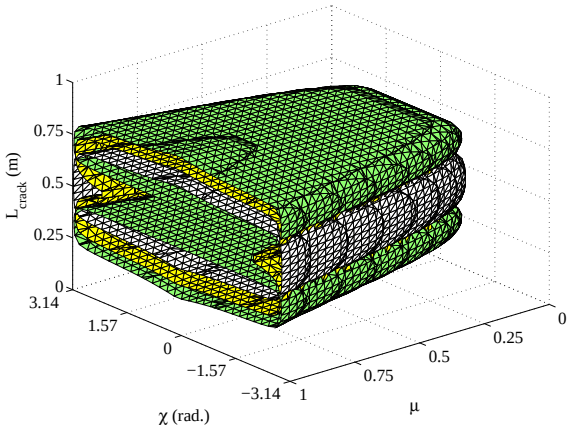

(b) Case 3, 1% noise level

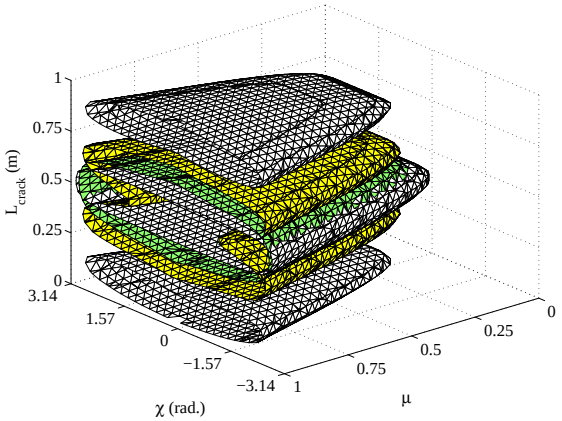

(c) Case 2, 2% noise level

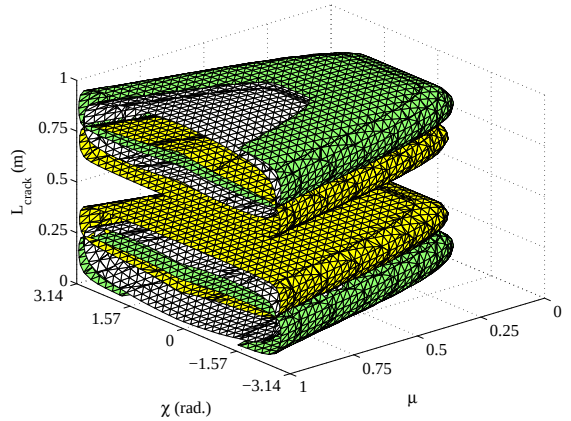

(d) Case 3, 2% noise level

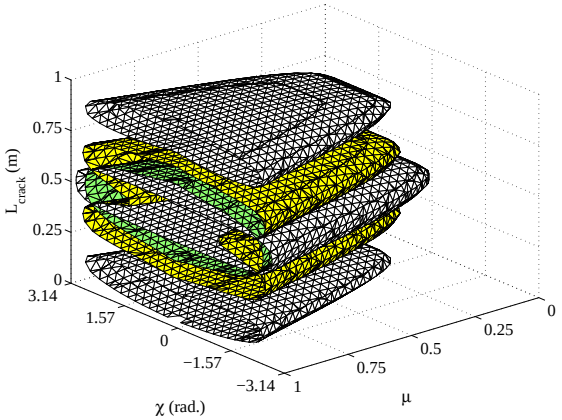

(e) Case 2, 4% noise level

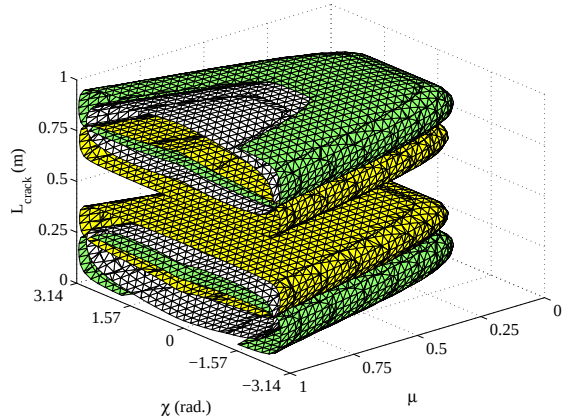

(f) Case 3, 4% noise level

Figure 17 : Surfaces $\%\Psi_{ij}^{cracked}$ with various noise levels for the case 2 ($\mu = 0.3$, $\chi = \frac{\pi}{5} rad.$ and $L_{crack} = 0.62m$) and the case 3 ($\mu = 0.5$, $\chi = \frac{2\pi}{3} rad.$ and $L_{crack} = 0.28m$) (green=$\%\Psi_{31}^{cracked}$,yellow=$\%\Psi_{51}^{cracked}$, white=$\%\Psi_{53}^{cracked}$)

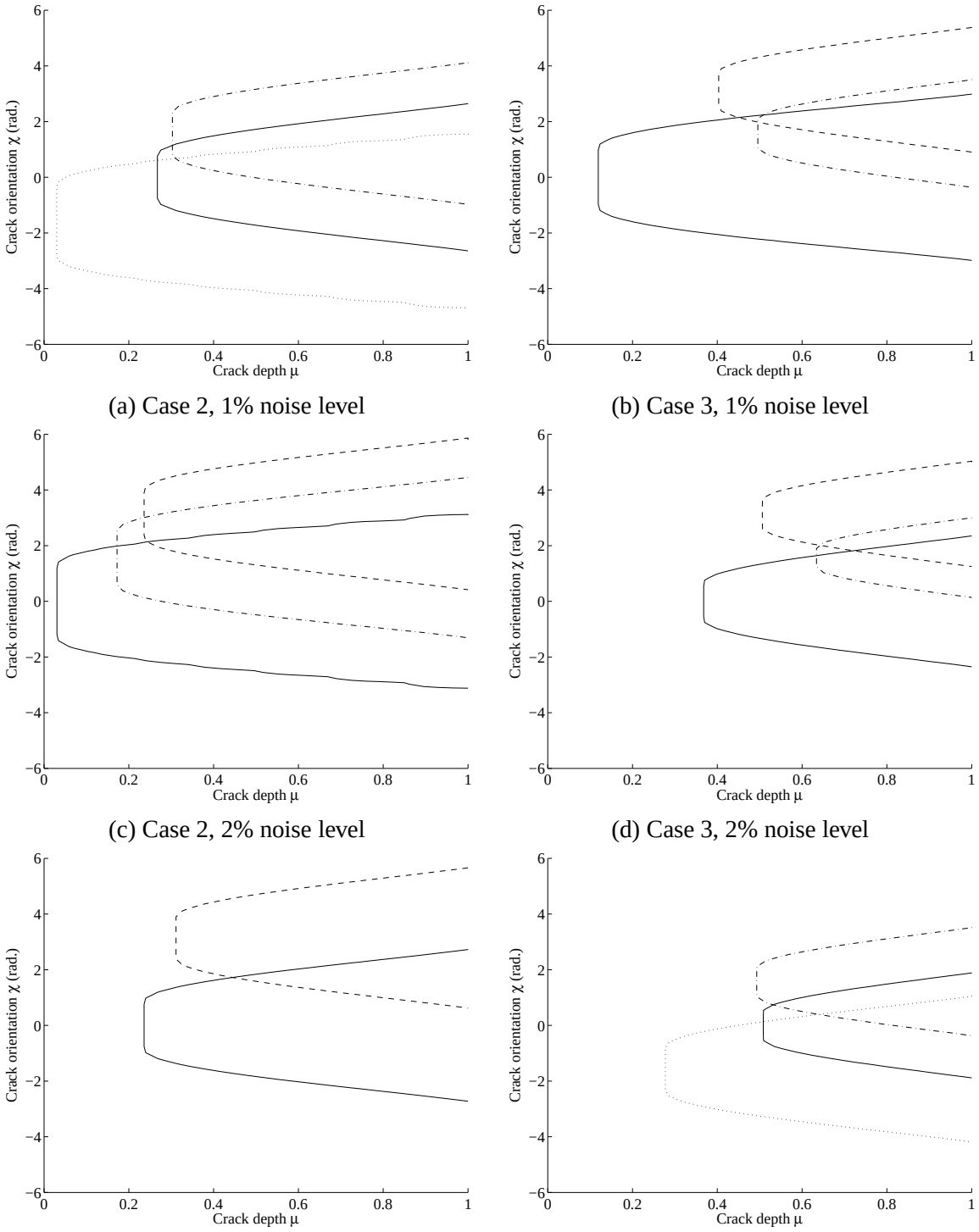

(a) Case 2, 1% noise level

(b) Case 3, 1% noise level

(c) Case 2, 2% noise level

(d) Case 3, 2% noise level

(e) Case 2, 4% noise level

(f) Case 3, 4% noise level

Figure 18 : Identification of the crack size μ and the crack orientation χ with various noise levels for the case 2 ($\mu = 0.3$, $\chi = \frac{\pi}{5} rad.$ and $L_{crack} = 0.62m$) and the case 3 ($\mu = 0.5$, $\chi = \frac{2\pi}{3} rad.$ and $L_{crack} = 0.28m$) and with the contour lines of $\%\Psi_{15}^{cracked}$ ($-\chi$, $-.-\chi+\frac{\pi}{2} rad.$, $--\chi+\pi rad.$, $\cdots\chi-\frac{\pi}{2} rad.$)

Table 5 : Evolution of the frequencies in Hz for the cases 1,2 and 3 without noise

Case	μ	L_{crack} (m)	$\chi(rad.)$	Angle (rad.)	f_1	f_2	f_3	f_4	f_5	f_6
1	0.8	0.15	$\frac{\pi}{3}$	χ	196.4	197.29	765.6	776.12	1699.54	1729.3
				$\chi+\pi/2$	194.99	197.09	749.47	773.73	1657.9	1722.35
				$\chi+\pi$	198.08	198.12	785.73	786.29	1758.4	1760.19
				$\chi-\pi/2$	198.63	198.63	792.64	792.65	1780.53	1780.58
2	0.3	0.62	$\frac{\pi}{5}$	χ	196.06	196.19	789.75	790	1783.66	1783.92
				$\chi+\pi/2$	196.17	196.29	789.98	790.2	1783.9	1784.13
				$\chi+\pi$	198.85	198.85	795.4	795.4	1789.66	1789.66
				$\chi-\pi/2$	198.74	198.74	795.17	795.17	1789.41	1789.41
3	0.5	0.28	$\frac{2\pi}{5}$	χ	198.09	198.09	790.62	790.66	1787.29	1787.31
				$\chi+\pi/2$	194.37	195.26	768.83	773.85	1776.77	1779.16
				$\chi+\pi$	195.39	195.84	774.62	777.21	1779.52	1780.76
				$\chi-\pi/2$	198.85	198.85	795.4	795.4	1789.66	1789.66

Table 6 : Evolution of the frequencies in Hz for the case 1 ($\mu = 0.8$, $\chi = \frac{\pi}{3} rad.$ and $L_{crack} = 0.15m$) and various noise levels

Noise (%)	Angle (rad.)	f_1	f_2	f_3	f_4	f_5	f_6
1	χ	196.3	196.64	769.19	775	1691.88	1733.71
	$\chi+\pi/2$	194.17	197.78	749.93	772.33	1655.82	1728.69
	$\chi+\pi$	198.72	197.22	786.49	789.83	1754.69	1767.03
	$\chi-\pi/2$	198.16	198.06	794.75	793.97	1773.96	1773.37
2	χ	196.8	197.7	768.04	771.2	1704.18	1717.9
	$\chi+\pi/2$	195.69	195.41	743.03	766.18	1648.85	1722.91
	$\chi+\pi$	198.62	197.22	785.77	793.34	1769.94	1774.89
	$\chi-\pi/2$	198.31	197.49	785.28	786.01	1769.19	1774.89
4	χ	196.42	196.68	770.51	781.51	1730.63	1707.98
	$\chi+\pi/2$	198.37	194.23	750.12	785.96	1687.23	1710.99
	$\chi+\pi$	198.37	196.07	778.69	790.71	1739.4	1772.96
	$\chi-\pi/2$	197.59	194.76	782.87	788.84	1763.03	1785.53
6	χ	194.35	195.87	742.63	758.95	1699.02	1681.4
	$\chi+\pi/2$	194.83	197.04	766.72	771.75	1687.66	1684.54
	$\chi+\pi$	194.52	193.22	774.38	791.47	1765.34	1772.01
	$\chi-\pi/2$	195.11	193.26	773.42	794.86	1737.36	1783.51
8	χ	196.2	194.23	778.75	793.62	1663.86	1687.2
	$\chi+\pi/2$	197.5	194.85	775.74	772.97	1603.65	1746.31
	$\chi+\pi$	194.51	190.9	760.2	780.63	1696.43	1711.87
	$\chi-\pi/2$	197.3	192.18	789.47	790.89	1765.1	1745.36
10	χ	197.3	193.03	755.71	742.33	1707.15	1787.47
	$\chi+\pi/2$	192.65	195.37	742.08	767.62	1637.5	1773.2
	$\chi+\pi$	195.76	193.23	773.38	794.4	1754.85	1737.01
	$\chi-\pi/2$	196.07	196.6	790.86	763.25	1777.66	1727.83

Table 7 : Evolution of the frequencies in Hz for the case 2 ($\mu = 0.3$, $\chi = \frac{\pi}{5} rad.$ and $L_{crack} = 0.62m$) and various noise levels

Noise (%)	Angle (rad.)	f_1	f_2	f_3	f_4	f_5	f_6
1	χ	195.45	196.4	787.46	793.94	1775.04	1782.85
	$\chi+\pi/2$	195.28	196.51	788.68	790.86	1776.87	1784.16
	$\chi+\pi$	198.5	197.95	791.52	793.32	1782.92	1781.92
	$\chi-\pi/2$	198.73	197.84	794.86	795.18	1789.27	1785.69
2	χ	196.94	198.04	792.98	794.77	1773.18	1781.91
	$\chi+\pi/2$	196.17	196.29	789.98	790.2	1783.9	1784.13
	$\chi+\pi$	197.23	197.81	788.86	792.12	1788.43	1773.39
	$\chi-\pi/2$	198.28	198.84	793.48	787.7	1780.91	1785.08
4	χ	196.46	193.95	794.98	783.96	1781.5	1784.34
	$\chi+\pi/2$	197.66	194.92	784.85	780.64	1776.84	1762.45
	$\chi+\pi$	196.34	196.54	794.99	792.14	1787.31	1789.15
	$\chi-\pi/2$	197.05	198.71	783.35	781.01	1767.32	1778.31

Table 8 : Evolution of the frequencies in Hz for the case 3 ($\mu = 0.5$, $\chi = \frac{2\pi}{3} rad.$ and $L_{crack} = 0.28m$) and various noise levels

Noise (%)	Angle (rad.)	f_1	f_2	f_3	f_4	f_5	f_6
1	χ	198.23	197.37	793.53	789.31	1787.08	1786.08
	$\chi+\pi/2$	194.02	194.33	767.72	775.74	1773.19	1773.48
	$\chi+\pi$	195.74	196.48	776.6	774.59	1780.45	1781.21
	$\chi-\pi/2$	198.63	198.76	792.83	795.18	1782.29	1787.24
2	χ	196.16	198.25	783.78	787.65	1781.57	1776.98
	$\chi+\pi/2$	193.61	193.36	761.22	781.4	1787.85	1788.78
	$\chi+\pi$	193.99	196.3	774.18	777.37	1774.01	1765.98
	$\chi-\pi/2$	198.23	198.68	791.35	788.12	1782.62	1772.95
4	χ	195.3	197.38	777.76	781.07	1786.23	1763.23
	$\chi+\pi/2$	194.6	195.29	768.32	770.06	1778.17	1768.16
	$\chi+\pi$	198.63	193.18	771.14	791.74	1748.68	1767.71
	$\chi-\pi/2$	194.89	195.77	786.36	780.12	1764.22	1768.72

various uniform random noise levels, respectively. The corresponding evolutions of the parameters $\%\Psi_{ij}^{cracked}$ are indicated in Tables 9, 10 and 11. Firstly, Figures 15 show the surfaces $\%\Psi_{31}^{cracked}$, $\%\Psi_{51}^{cracked}$ and $\%\Psi_{53}^{cracked}$ with various noise levels for case 1 ($\mu = 0.8$, $\chi = \frac{\pi}{3}$ and $L_{crack} = 0.15m$). Table 12 gives the estimated crack location that corresponds to the centroid of the three surfaces. Due to the presence of noise measurement, the three surfaces do not intersect in an unique line. However, the centroid of the crack location that is given in Table 12 indicates that the crack location is correctly identified even if noise level have been added in the numerical simulations. Then, it may be noted that the non-uniqueness of the crack location may always be avoid by considering the driving point Frequency Response Function that is characterized by a successive change in the resonances and antiresonances even if noise level has been added on the numerical simulations (see Section 3.2).

Secondly, Figures 16 illustrate the contour lines of $\%\Psi_{15}^{cracked}$ and the corresponding identification of the crack size μ and the crack orientation χ with various noise levels. Due to the presence of measurements errors, the intersection of the three curves does not exist. However, the centroid of the different pairs of intersections may be taken as the crack position and crack size when the three curves do not meet exactly. Considering the re-

Table 9 : Values of $\%\Psi_{ij}^{cracked}$ for the case 1 ($\mu = 0.8$, $\chi = \frac{\pi}{3} rad.$ and $L_{crack} = 0.15m$) and various noise levels

Noise (%)	Angle (rad.)	$\%\Psi_{31}^{cracked}$	$\%\Psi_{51}^{cracked}$	$\%\Psi_{53}^{cracked}$
1	χ	8.167	38.138	5.044
	$\chi+\pi/2$	13.782	47.244	4.204
	$\chi+\pi$	4.214	16.992	1.897
	$\chi-\pi/2$	-1.063	4.788	1.791
2	χ	9.745	34.075	3.113
	$\chi+\pi/2$	20.296	57.404	3.092
	$\chi+\pi$	4.393	8.901	-0.249
	$\chi-\pi/2$	4.018	7.876	-0.294
4	χ	7.721	18.909	0.392
	$\chi+\pi/2$	21.868	49.468	0.07
	$\chi+\pi$	7.45	23.136	1.624
	$\chi-\pi/2$	3.784	7.717	-0.201
6	χ	17.886	25.788	-3.783
	$\chi+\pi/2$	6.467	33.782	4.887
	$\chi+\pi$	1.901	-7.537	-2.967
	$\chi-\pi/2$	3.588	9.532	0.368
8	χ	3.078	51.95	11.343
	$\chi+\pi/2$	7.221	88.027	18.275
	$\chi+\pi$	9.179	27.856	1.843
	$\chi-\pi/2$	-0.13	5.386	1.419
10	χ	16.976	34.742	-0.902
	$\chi+\pi/2$	14.812	50.028	4.336
	$\chi+\pi$	4.928	3.558	-1.906
	$\chi-\pi/2$	-3.361	-6.652	0.226

Table 10 : Values of $\%\Psi_{ij}^{cracked}$ for the case 2 ($\mu = 0.3$, $\chi = \frac{\pi}{5} rad.$ and $L_{crack} = 0.62m$) and various noise levels

Noise (%)	Angle (rad.)	$\%\Psi_{31}^{cracked}$	$\%\Psi_{51}^{cracked}$	$\%\Psi_{53}^{cracked}$
1	χ	-2.897	-8.185	-0.413
	$\chi+\pi/2$	-3.865	-9.897	-0.297
	$\chi+\pi$	1.24	1.781	-0.253
	$\chi-\pi/2$	0.031	-0.35	-0.105
2	χ	-2.65	-0.358	1.392
	$\chi+\pi/2$	1.969	-4.246	-2.18
	$\chi+\pi$	0.027	-6.782	-1.711
	$\chi-\pi/2$	-0.175	1.832	0.556
4	χ	-4.644	-6.779	0.907
	$\chi+\pi/2$	2.921	1.043	-1.393
	$\chi+\pi$	-4.909	-10.322	0.179
	$\chi-\pi/2$	2.469	3.129	-0.61

Table 11 : Values of $\%\Psi_{ij}^{cracked}$ for the case 3 ($\mu = 0.5$, $\chi = \frac{2\pi}{3} rad.$ and $L_{crack} = 0.28m$) and various noise levels

Noise (%)	Angle (rad.)	$\%\Psi_{31}^{cracked}$	$\%\Psi_{51}^{cracked}$	$\%\Psi_{53}^{cracked}$
1	χ	-0.299	-1.496	-0.206
	$\chi+\pi/2$	4.313	-13.909	-5.968
	$\chi+\pi$	3.246	-9.606	-4.262
	$\chi-\pi/2$	0.847	2.702	0.2
2	χ	0.437	-8.227	-2.305
	$\chi+\pi/2$	6.833	-23.421	-9.868
	$\chi+\pi$	0.917	-14.491	-4.148
	$\chi-\pi/2$	0.797	0.74	-0.264
4	χ	1.757	-14.615	-4.662
	$\chi+\pi/2$	5.171	-13.774	-6.435
	$\chi+\pi$	11.763	19.615	-1.765
	$\chi-\pi/2$	-3.488	-5.24	0.646

Table 12 : Estimation of the crack location for cases 1, 2 and 3 with various noise levels

Case	Noise (%)	$L_{crack}(m)$
1	1	0.13
	2	0.16
	4	0.2
	6	0.22
	8	0.18
	10	0.2
2	1	0.63
	2	0.6
	4	0.6
3	1	0.38
	2	0.24
	4	0.24

sults presented in Figures 16, it may be concluded that measurement errors and uncertainties on the frequencies inevitably degrade the accuracy in practical cases. Effectively, the area defines by the intersections of the different curves $\%\Psi_{15}^{cracked}$ for the various shaft rotoations increase when the noise measurement increase. However, the identifications of all the crack parameters (location, size and orientation) are obtained with satisfactory precisions even if 1%, 2%, and 4% uniformly distributed random noise level is added to the simulations. If the noise level is greater that 6%, the identification of the crack size and orientation may be more difficult. Moreover, it may be observed that the crack depth and orientation has been detected with less accuracy than the crack position. Finally, it may be noted that the use of $\%\Psi_{13}^{cracked}$ and/or $\%\Psi_{35}^{cracked}$ could allow to undertake an additionnal damage identification of the crack size and orientation in orde to confirm the previous identification with $\%\Psi_{15}^{cracked}$. In conclusion, the quality of the experimental data that is an important key in achieving reliable identification with the RFSI-method.

Now, the sensibility of the RFSI-method and robust identification of the crack parameters is undertaken for cases 2 and 3 that correspond to the presence of "'small"' cracks. The identification of the crack location and the corresponding results of the surfaces $\%\Psi_{31}^{cracked}$, $\%\Psi_{51}^{cracked}$ and $\%\Psi_{53}^{cracked}$ with 1%, 2% and 4% noise levels are presented in Figures 17. The associated results for the identification of the crack size and orientation are given in Figures 18. Moreover, it clearly appears that

the crack location, orientation and size may be evaluated by considering the centroid of the surfaces $\%\Psi_{ij}^{cracked}$ and the different curves $\%\Psi_{15}^{cracked}$ for the four shaft rotations. However, it appears that the identification of the crack parameters is not possible if the noise level is more than 2% (see Figures 17(e) and (f)). So it may be concluded that the quality of the measurements for the identification of a small crack is an important factor to take into account for a robust identification of the crack location, size and orientation by using the RFSI-method.

In conclusion, the identification of the crack parameters can be less or more difficultly obtained depending on the effect of uncertainties due to measurement errors and environmental conditions and the characteristics of the crack. However, if 1% or 2% uniformly distributed random noise level is added to the numerical simulations, the Frequencies' Ratio Surfaces Intersection method (FRSI-method) can be used for the detection of the crack size, location and orientation with satisfactory precision.

Conclusion

Two new criterions $\%\Delta_i^{cracked}$ and $\%\Psi_{i,j}^{cracked}$ and the Frequencies' Ratio Surfaces Intersection method are given in order to identify the non-dimensional crack depth, the crack location and the crack orientation. The FRSI-method considers the intersection of the surfaces that correspond to the natural frequencies' ratio of the lower modes. It is demonstrated that a robust identification of the crack parameters is possible by only using the natural frequencies of the cracked beam. Moreover, an accurate knowledge of the material properties (i.e. the Young modulus and the density) is not required. The non-uniqueness of the crack size location that is classically observed for structural symmetric beams when the Frequencies' Ratio Surfaces Intersection method method is used, may be avoid by only considering the emerging of extra antiresonances on the Frequency Response Function of the crack beam.

The proposed methodology was numerically validated in the case of a simply supported beam with various crack locations, depths and orientations. The obtained results demonstrate that a certain level of accuracy for the measured data is needed in order to allow a correct damage detection. Moreover, the procedure developed here works effectively only for measurement errors not exceeding 2% for small levels of crack depth. So it may be concluded that the quality of the experimental data is an important key in order to achieve reliable results due to the fact that the presence of experimental errors and uncertainties may produce a modification in the identification of the crack size and orientation.

Finally, the proposed methodology and the generalized criterion $\%\Psi_{i,j}^{cracked}$ has the potential as a damage detection technique for rectangular cross section beams or more complex structures.

References

Adams, R.; Cawley, P.; Pye, C.; Stone, B. (1978): "A vibration technique for non-destructively assessing the integrity of structures". *Journal of Mechanical Engineering Science,* **20**, pp. 93–100.

Bamnios, Y.; Douka, E.; Trochidisi, A. (2002): "Crack identification in beam structures using mechanical impedance". *Journal of Sound and Vibration,* **256 (2)**, p. 287–297 .

Cerri, M. N.; Vestroni, F. (2000): "Detection of damage in beams subjected to diffused cracking". *Journal of Sound and Vibration,* **234(2)**, pp. 259–276.

Davies, W. G. R.; Mayes, I. W. (1984): "The vibrational behaviour of a multi-shaft, multi-bearing system in the presence of a propagating transverse crack". *Transactions of the ASME Journal of Vibration, Acoustics, Stress, and Reliability in Design,* **106**, pp. 146–153.

Dharmaraju, N.; Sinha, J. K. (2005): "Some comments on use of antiresonance for crack identification in beams". *Journal of Sound and Vibration,* **286**, p. 669–671 .

Dharmaraju, N.; Tiwari, R.; Talukdar, S. (2004): "Identification of an open crack model in a beam based on force response measurements". *Computers and Structures*, **82**, p. 167–179 .

Dharmaraju, N.; Tiwari, R.; Talukdar, S. (2005): "Development of a novel hybrid reduction scheme for identification of an open crack model in a beam". *Mechanical Systems and Signal Processing,* **19**, p. 633–657 .

Dilena, M.; Morassi, A. (2002): "Identification of crack location in vibrating beams from changes in node posi-

tions". *Journal of Sound and Vibration,* **255(5)**, pp. 915–930.

Dilena, M.; Morassi, A. (2004): "The use of antiresonances for crack detection in beams". *Journal of Sound and Vibration,* **276**, p. 195–214 .

Dimarogonas, A. (1996): "Vibration of cracked structures: a state of the art review". *Applied Mechanics Review,* **55**, pp. 831–857 .

Doebling, S.; Farrar, C.; Prime, M. (1998): "A summary review of vibration-based damage identification methods.". *The Shock and Vibration Digest,* **30(2)**, pp. 91–105 .

Douka, E.; Bamnios, G.; Trochidis, A. (2004): "A method for determining the location and depth of cracks in double-cracked beams". *Applied Acoustics,* **65**, p. 997–1008 .

Gasch, R. (1993): "A survey of the dynamic behaviour of a simple rotating shaft with a transverse crack". *Journal of Sound and Vibration,* **160(2)**, pp. 313–332.

Gladwell, G.; Morassi, A. (1999): "Estimating damage in a rod from changes in node positions". *Inverse Problems in Engineering,* **7**, pp. 215–233.

Harris, C.; Piersol, A. G. (2002): *Harris' shock and vibration handbook*, 5 ed. McGraw-Hill.

Hearn, G.; Testa, R. (1991): "Modal analysis for damage detection in structures". *American Society of Civil Engineers, Journal of Structural Engineering,* **117**, pp. 3042–3063.

Khiema, N.; Lien, T. (2004): "Multi-crack detection for beam by the natural frequencies". *Journal of Sound and Vibration,* **273**, p. 175–184 .

Lalanne, M.; Ferraris, G. (1990): *Rotordynamics Prediction in Engineering*, 2 ed. John Wilet and Sons.

Li, B.; Chen, X.; Ma, J.; He, Z. (2005): "Detection of crack location and size in structures using wavelet finite element methods". *Journal of Sound and Vibration,* **285**, p. 767–782 .

Liang, R.; Hu, J.; Choy, F. (1992): "Theoretical study of crack-induced eigenfrequency changes on beam structures". *American Society of Civil Engineers, Journal of Engineering Mechanics,* **118(2)**, pp. 384–396.

Mayes, I. W.; Davies, W. G. R. (1984): "Analysis of the response of a multi-rotor-bearing system containing a transverse crack in a rotor". *Transactions of the ASME Journal of Vibration, Acoustics, Stress, and Reliability in Design,* **106**, pp. 139–145.

Morassi, A. (1993): "Crack-induced changes in eigenparameters of beam structures". *American Society of Civil Engineers, Journal of Engineering Mechanics,* **119**, pp. 1798–1803.

Nahvi, H.; Jabbari, M. (2005): "Crack detection in beams using experimental modal data and finite element model". *International Journal of Mechanical Sciences,* **47**, p. 1477–1497 .

Nelson, H.; Nataraj, C. (1986): "The dynamics of a rotor system with a cracked shaft". *Journal of Vibration, Acoustics, Stress and Reliability in Design,* **108**, p. 189–196.

Owolabi, G.; Swamidas, A.; Seshadri, R. (2003): "Crack detection in beams using changes in frequencies and amplitudes of frequency response functions". *Journal of Sound and Vibration,* **265**, pp. 1–22.

Sinou, J.-J. (2007): "Numerical investigations of a robust identification of crack location and size in beams using only changes in ratio pulsations of the cracked beams". *Structural Engineering Mechanics,* **25(6)**, pp. 691–716.

Sinou, J.-J.; Lees, A. W. (2005): "Influence of cracks in rotating shafts". *Journal of Sound and Vibration,* **285(4-5)**, pp. 1015–1037.

Swamidas, A.; Yang, X.; Seshadri, R. (2004): "Identification of cracking in beam structures using timoshenko and euler formulations". *Journal of Engineering Mechanics,* **130(11)**, pp. 1297–1308.

Wahl, F.; Schmidt, G.; Forrai, L. (1996): "On the significance of antiresonance frequencies in experimental structural analysis". *Journal of Sound and Vibration,* **219 (3)**, p. 379–394 .

Wauer, J. (1990): "Dynamics of cracked rotors: Literature survey". *Applied Mechanics Review,* **43**, pp. 13–17 .